ACS Sustainable Chemistry & Engineering

pubs.acs.org/journal/ascecg

Research Article

From CO_2 to Sustainable Aviation Fuel: Navigating the Technology Landscape

Pussana Hirunsit,* Alessandro Senocrate, Carlos E. Gómez-Camacho, and Florian Kiefer*

Cite This: https://doi.org/10.1021/acssuschemeng.4c03939

Read Online

ACCESS | Metrics & More | Article Recommendations | Supporting Information

ABSTRACT: Sustainable jet fuel plays a crucial role in reducing aviation's carbon footprint, offering a promising approach toward net-zero emissions in the aviation sector. This work investigates pathways for producing jet fuels directly from CO_2. Given the early stage of many direct CO_2 utilization technologies, identifying promising pathways is essential. Our investigation focuses on the three most important routes for jet fuel production, each of which employs a distinct intermediate compound. These routes are the reverse water−gas shift and Fischer−Tropsch (RWGS-FT) route, the methanol route, and the CO_2 electrolysis route, which employ syngas, methanol, and ethylene as key intermediates, respectively. By performing comprehensive process simulations and analyzing the resulting energy intensity and thermal and CO_2 efficiency of each route, these findings provide quantitative early-stage evaluations and allow us to identify key technical development requirements. Our results indicate that the methanol route exhibits the lowest energy intensity, followed by the RWGS-FT and CO_2 electrolysis routes. H_2 production accounts for a significant share of the energy demand for the RWGS-FT and methanol routes. The RWGS-FT route shows the lowest CO_2 efficiency, while the methanol route achieves 92% CO_2 efficiency including recycle streams, highlighting its potential for jet fuel production. Furthermore, the CO_2 electrolysis route holds the potential to achieve close to 100% CO_2 efficiency and requires significantly less H_2 feedstock. However, it faces challenges of a high energy demand. In addition, our study investigates key effects of potential technology optimization, providing a guideline for research and technology optimization.

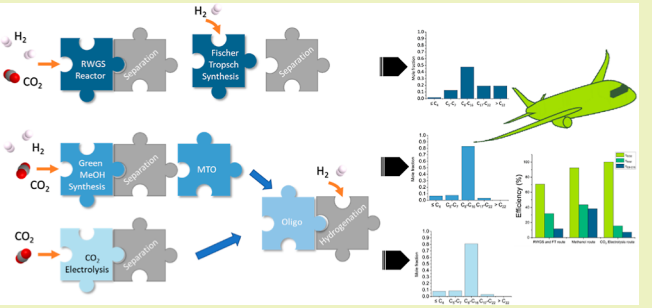

KEYWORDS: *sustainable aviation fuels, process simulation, reverse water gas shift, Fischer-Tropsch, methanol-to-olefins, CO_2 electrolysis, oligomerization*

1. INTRODUCTION

Today, the aviation sector alone accounts for 2.5% of global CO_2 equivalent emissions. With demands increasing by 4% annually, technical efforts to reduce fuel consumption are currently largely insufficient.[1] Airlines, as per International Air Transport Association,[2] have committed to achieve net-zero CO_2 emissions by 2050, with sustainable aviation fuel (SAF) seen as a key contributor and expected to account for 65% of the mitigation strategy. To align with the net zero goal, SAF production must reach at least 46 million tonnes by 2030 and 360 million tonnes by 2050.[2,3] Despite this, only 0.5 million tonnes of SAF were produced in 2023.[3] Moreover, current certified SAF production pathways predominantly utilize feedstock derived from biomass and waste,[4] in contrast to regulatory changes, emphasizing the need for nonbiogenic SAF to circumvent the limited availability of biomass (2023 EU RED-III[5] and ReFuelEU Aviation Regulation[6]). Therefore, alternative carbon sources derived from CO_2 are becoming increasingly important for SAF production, given their abundance and potential for CO_2 mitigation. Within the requirement of using a CO_2-based feedstock as well as renewable electrical energy to power the conversion, we identify three key pathways for producing liquid hydrocarbons suitable for jet fuels. Jet fuels primarily consist of hydrocarbons within the C_8−C_{16} range, which are crucial for optimal performance and efficiency in aviation engines. The key catalytic processes in the three studied pathways are at both low and high technology readiness level (TRL) and proceed through different key intermediates: (i) the RWGS-FT pathway making use of reverse water gas shift (RWGS) to produce syngas (CO + H_2) as a key intermediate, coupled with the Fischer−Tropsch (FT) synthesis, (ii) the methanol pathway converting CO_2 to CH_3OH as a key intermediate, followed by the methanol-to-olefins (MTO) and olefins oligomerization processes, and (iii) the CO_2 electrolysis

Received: May 13, 2024
Revised: July 10, 2024
Accepted: July 10, 2024

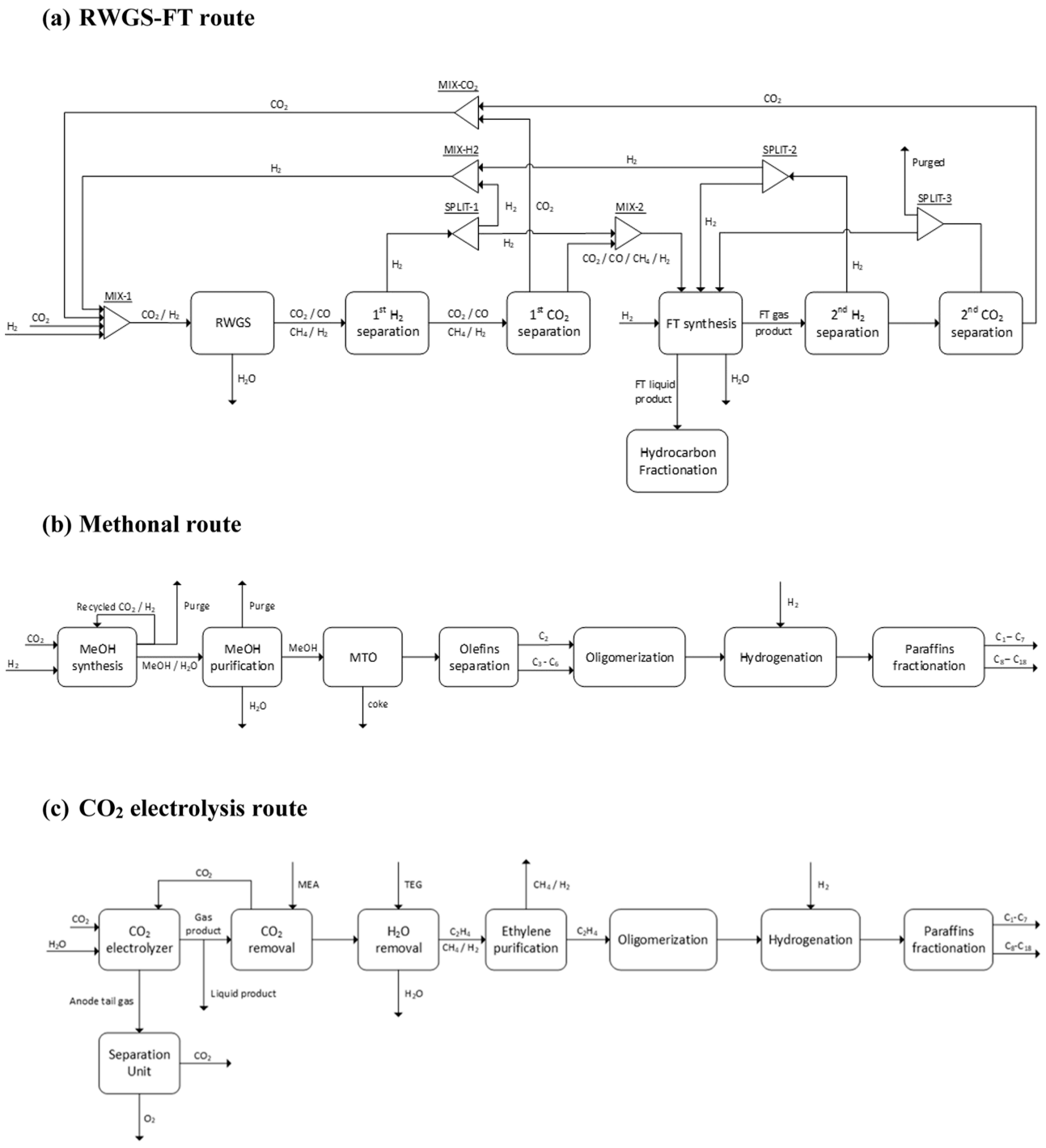

Figure 1. Conceptual process diagrams for converting CO_2 into liquid hydrocarbon within the C_8−C_{16} range using three pathways: (a) RWGS-FT route, (b) methanol route, and (c) CO_2 electrolysis route.

pathway, exploiting the direct electrochemical reduction of CO_2 to C_2H_4 as a key intermediate, later fed to the olefins oligomerization process. To identify promising routes among these key emerging candidates, it is essential to evaluate how both current and prospective developments could influence the applicability of these technologies as a subprocess for jet fuel production.

Currently, the FT process utilizing syngas derived from biomass, waste, or biocrude feedstock is one of the certified processes for SAF production,[4] in which the FT products can be further upgraded through oligomerization of C_3−C_4, hydrotreating, aromatization, and hydrocracking to produce fully formulated jet fuels.[7] This makes the RWGS-FT pathway a benchmark for comparison in this work. Coupling the FT synthesis with syngas production processes using sustainable CO_2 sources, such as RWGS reaction or CO_2 electrolysis, critically influences the efficiency of the overall pathway and the FT process.[8,9] Previous studies have shown that coupling high-temperature co-electrolysis for syngas production with FT synthesis and upgrading can achieve a power-to-liquid efficiency of 46% for combined synthetic diesel and kerosene production.[10] While the high energy requirement for the

https://doi.org/10.1021/acssuschemeng.4c03939
ACS Sustainable Chem. Eng. XXXX, XXX, XXX−XXX

endothermic RWGS reaction currently limits its industrial applicability,[11,12] this work aims to elucidate how the RWGS process affects the efficiency of the overall production process, which is crucial for optimizing the pathway.

The second route from CO_2 over CH_3OH as an intermediate is compelling due to the ease of transportation and storage of methanol and its potential as a platform chemical. While subprocesses such as MTO and methanol-to-gasoline (MTG) are established in large-scale industrial application, a process chain converting methanol to jet fuel has not yet been demonstrated at the industrial scale.[13−15]

Furthermore, the direct electrochemical reduction of CO_2 to C_2H_4 has shown promising results at the laboratory scale[16−18] and is considered a subprocess in the third route. This technology is still in an early stage of development, with low TRL. However, it has been reported that enhancing certain short-term technical and economic factors could make direct CO_2 electrolysis a more profitable method for C_2H_4 production.[19] Therefore, the pathway through the C_2H_4 intermediate produced by direct CO_2 electrolysis is also compelling and, thus, selected for further investigation.

This study focuses on evaluating the three pathways applied for the production of liquid hydrocarbons in the C_8−C_{16} range, key components of jet fuels, using CO_2 as a feedstock. It specifically examines these hydrocarbons without considering downstream processes to upgrade them to fully formulated jet fuels. Our approach leverages early-stage, limited, and lab-scale data to compare the production pathways based on criteria such as electrical-to-fuel efficiency and carbon efficiency. We use comprehensive process modeling, heat integration analysis, and sensitivity analysis to pinpoint crucial technical development needs and assess the realistic potentials of the chemical conversion technologies involved in each pathway. The simulations incorporate kinetic models and appropriate separation techniques to develop scalable and robust processes.

Our findings identify the methanol pathway as having the lowest energy intensity, followed by RWGS-FT and CO_2 electrolysis routes. Additionally, the methanol route can achieve relatively high thermal and CO_2 efficiency compared with the other two pathways. The study also explores potential technology improvements, examining the impact of reducing the CO_2 electrolyzer cell voltage and altering the CO_2 conversion rate in the CO_2 electrolysis route, catalyst coking in the MTO process for the methanol route, and the absence of heat recovery from off-gas combustion in the RWGS-FT pathway on energy and CO_2 efficiency. Ultimately, this research intends to provide valuable insights and guidance to decision-makers in research and development, serving as a benchmark for evaluating the impact of novel and optimized technologies in the aviation fuel sector.

2. METHOD AND PROCESS DESCRIPTION

This section outlines the three distinct investigated routes for converting CO_2 into liquid hydrocarbon aviation fuel within the C_8−C_{16} range. Each route has been modeled by considering a series of steps integrating downstream separation processes for key intermediates and the recycling of CO_2 and H_2 reactants. Each pathway uses distinct intermediary molecules in the conversion of CO_2 to hydrocarbons, i.e., syngas (CO + H_2), CH_3OH, and C_2H_4. The CO_2 feedstock source and the energy demand to procure the CO_2 are beyond the scope of this analysis as the primary focus of this work is on the effectiveness of the transformation process of CO_2 into liquid hydrocarbons. CO_2 can be provided by direct air capture or other point source carbon capture technologies. Nevertheless, this study accounts for the energy demand for the feedstock green H_2 produced by water electrolysis as there is a significant trade-off between its use in the RWGS-FT route and methanol synthesis but not in CO_2 electrolysis.

The modeling and simulation of the processes are conducted using Aspen Plus V12.1 software. Certain modeling parameters are established to be consistent across all three processes, as outlined in Section S1 of the Supporting Information. Most reactor modeling incorporates kinetic models from the literature to provide reliable estimates for conversion and product distributions based on the current state-of-the-art. Depending on the reaction type and available data, some reactors are modeled based on the assumption of the chemical equilibrium or using yield data from published experimental studies. This is due to unavailable data of the proper kinetic models for implementation into Aspen Plus. Catalyst regeneration steps are not included in the simulation but are considered in the analysis. The separation techniques for intermediate compounds are chosen based on stream composition and on the suitability for scalability to develop robust and realistic processes. The size selection has been done arbitrarily, corresponding to an upscaling in production. The proper size determination would require a further techno-economic assessment, which is not included in this work. While the simulations in this study are not fully optimized, which might result in an overestimation in the energy requirement, the observed trends offer valuable insights and suggest avenues within each route for reducing energy demand and enhancing the process efficiency.

2.1. Reverse Water Gas Shift and Fischer−Tropsch Route. The RWGS-FT route comprises four main stages: (1) the RWGS reaction for syngas production, (2) the first CO_2 and H_2 separation, (3) the FT synthesis for hydrocarbon fuel production, and (4) the second CO_2 and H_2 separation. Figure 1a provides a conceptual process diagram, while a detailed process flow diagram of each unit can be found in Section S2.1 of the Supporting Information.

The FT process produces a crude, which is analyzed based on its composition in the work at hand. Downstream upgrading of this syncrude can enhance the overall conversion toward the targeted products, in this case hydrocarbons in the C_8−C_{16} range. Various designs of this process exist. For example, Atsonios et al.[20] proposed that after the FT synthesis reactor, the products are sent to CO_2 and H_2 removal units. Downstream, light gases and hydrocarbons are separated; olefins are recompressed and sent to an oligomerization reactor. The products go to a flash drum to separate light gases and olefins, with the gases sent to an autothermal reactor (ATR) for reforming into syngas. Both olefins and hydrocarbons then undergo hydrotreatment to form paraffins. Heavy paraffins are hydrocracked into smaller paraffins. After hydrocracking, hydrocarbons are sent to a H_2 removal unit and then to a distillation column where light hydrocarbons are taken at the top and sent to the ATR, while heavy hydrocarbons at the bottom are sent to a second distillation column where kerosene is taken at the top and diesel at the bottom. The FT downstream process proposed by Bube et al.[21] involves recycling and partially purging light gases (mainly H_2, CO, CH_4, and CO_2) to provide process heating, and hydrocarbons are separated into fractions of $C_{<8}$ and $C_{\geq 8}$, followed by hydrotreating. Heavy hydrocarbons (waxes) are

https://doi.org/10.1021/acssuschemeng.4c03939
ACS Sustainable Chem. Eng. XXXX, XXX, XXX−XXX

sent to hydrocracking and then fractionated into different fuel fractions: light gases, naphtha (C_5−C_7), kerosene (C_8−C_{16}), and diesel (C_{17}−C_{20}). In addition, further steps of isomerization and aromatization may be required to upgrade hydrocarbons to aviation-grade kerosene. In this work, the downstream processes of the FT product upgrade are not included in the simulation. This study aims to focus solely on the conventional C_8−C_{16} liquid products produced by the FT synthesis without biasing the results by the additional process design for the FT product upgrade.

2.1.1. RWGS Reaction. Syngas, a mixture of primarily CO and H_2, is a key intermediate in this route and is produced by the RWGS reaction (Reaction 1). The RWGS reaction is thermodynamically favorable at high temperatures. Operating the RWGS reactor at temperatures below 600 °C may lead to methanation (Reactions 2 and 3).[22] Additionally, the formation of solid carbon via CO dissociation, which is favored at low temperature (Boudouard reaction, $\Delta H^0 = -171$ kJ/mol) and CH_4 dissociation, which is favored at higher temperature ($\Delta H^0 = +75$ kJ/mol), can occur, resulting in coke poisoning.[23] These side reactions adversely affect the RWGS reactivity. Hence, one of the significant challenges in RWGS technology is to conduct the process at lower temperatures to minimize energy consumption while avoiding undesired methanation reaction. Many studies have focused on exploring the RWGS reaction over catalysts based on metals such as Ni, Ru, Cu, Fe, and Pt, typically supported on metal oxides like Al_2O_3, SiO_2, or CeO_2.[24−26] Nickel is considered a suitable catalyst for the RWGS reaction due to its low cost and high catalytic activity.[24] On the other hand, using supports can significantly impact performance in terms of conversion and product selectivity.[25] It has also been reported that Ni supported on CeO_2 can enhance RWGS performance.[25,27,28]

Many studies report various operating conditions for the RWGS reaction, such as temperatures ranging from 250 to 700 °C, CO_2/H_2 feed ratios, and gas hourly space velocity, depending on the catalyst choice.[12] To simulate the reaction without a strong dependence on catalyst choice and its corresponding suitable operating temperature, which significantly impacts the energy requirements of the RWGS unit, the RWGS reactor (R-RWGS) is modeled using the RGibbs model reactor. This model assumes that the RWGS reaction reaches equilibrium following the Gibbs free energy minimization approach. In addition, to mitigate CO_2-methanation, the RWGS reactor is simulated operating at 800 °C and atmospheric pressure, similar to the conditions implemented by Hannula et al.[8] The equilibrium compositions at 800 °C are approximately 25% CO, 25% H_2O, 28% CO_2, 23% H_2, and less than 0.01% CH_4, which is consistent with findings reported by Chen et al.[29]

The CO_2 and H_2 feed gases are preheated to 650 °C (HEATER-1) before entering the RWGS reactor, and the product stream is cooled to 5 °C to remove condensable byproducts. The detailed process flow diagram for the RWGS process is provided in Section S2.1 of the Supporting Information.

$$CO_2 + H_2 \leftrightarrow CO + H_2O \quad \Delta H^0 = +41.2 \text{ kJ/mol} \tag{1}$$

$$CO + 3H_2 \leftrightarrow CH_4 + H_2O \quad \Delta H^0 = -206 \text{ kJ/mol} \tag{2}$$

$$CO_2 + 4H_2 \leftrightarrow CH_4 + 2H_2O \quad \Delta H^0 = -165 \text{ kJ/mol} \tag{3}$$

2.1.2. First H_2 and CO_2 Separation. Prior to entering the FT reactor, unreacted CO_2 and H_2 gases are separated. The output stream from the RWGS reactor contains a relatively large amount of unreacted H_2 and CO_2, approximately 23 mol % H_2 and 23 mol % CO_2. It is essential to separate H_2 and CO_2 for recycling and to control the amount of H_2 fed to the FT reactor before entering the FT reactor, as CO_2 capture and H_2 production by water electrolysis are quite energy-intensive, and the H_2/CO ratio fed to the FT reactor is also a crucial operative parameter.

Pressure swing adsorption (PSA) (H_2-SEP-1), a well-established industrial process for H_2 separation using molecular sieve as adsorbent, is considered operating at 40 bar and 25 °C achieving 85% H_2 recovery with 99.999 mol % purity.[9] This H_2 stream is mainly directed to the FT reactor, with a small split fraction being recycled to the RWGS reactor. A 2:1 molar ratio of H_2/CO entering the FT reactor (R-FT) is controlled, which is crucial for optimal FT liquid production. Subsequently, the process stream undergoes CO_2 membrane separation (CO_2-SEP-1) at 13 bar and 35 °C, recovering 80% of unreacted CO_2 with close to 100 mol % purity.[30] The recovered CO_2 is then recycled to the RWGS reactor.

2.1.3. FT Synthesis. FT synthesis, a highly exothermic process, converts syngas into a diverse range of hydrocarbon products, primarily *n*-paraffins (Reaction 4) and 1-olefins (Reaction 5). Oxygenates and aromatics are also produced but in a much smaller amount. Operating temperatures between 210 and 240 °C should be maintained to maximize the production of high-molecular-weight linear alkanes.[31] A slurry-bed reactor is preferred for improved temperature control and conversion efficiency.[31] In this work, the kinetic model proposed by Todic et al.[32] is implemented to simulate the major product distribution characteristic of *n*-paraffin and 1-olefins up to C_{30}, based on kinetic experiments performed on a rhenium-promoted Co/Al_2O_3 catalyst using the Langmuir−Hinshelwood−Hougen−Watson (LHHW) approach and carbide FT synthesis mechanism.[32] Detailed information regarding the kinetic model can be found in Section S2.3 of the Supporting Information. Product distribution from the FT synthesis with conventional catalysts predominantly yields *n*-paraffins and 1-olefins, with iso-paraffin production being relatively small, ranging from 0.1 to 1% in the C_5−C_{15} range, depending on the catalyst and promoter species.[33] To the best of our knowledge, a kinetic model that accurately describes FT product distribution including all paraffins and olefins and that can be implemented into the simulation is not available. Therefore, given the less than 1% production of isoparaffins and the absence of a comprehensive kinetic model, isoparaffins are not included as products in the FT synthesis for this work.

The FT reactor (R-FT) is modeled using a CSTR reactor model, operating at 220 °C and 25 bar with a 2:1 H_2/CO feed molar ratio, resulting in 52% CO conversion and a product distribution of *n*-paraffins and 1-olefins consistent with that reported by Todic et al.,[32] as shown in Figure S2.7 in the Supporting Information. Make-up H_2 gas is required at the FT reactor to keep a 2:1 molar ratio of H_2/CO entering the FT reactor.

$$nCO + (2n + 1)H_2 \leftrightarrow C_nH_{2n+2} + nH_2O \tag{4}$$

$$nCO + 2nH_2 \leftrightarrow C_nH_{2n} + nH_2O \tag{5}$$

The catalyst regeneration unit is not included in the process simulation for simplification purposes. However, it is important

https://doi.org/10.1021/acssuschemeng.4c03939
ACS Sustainable Chem. Eng. XXXX, XXX, XXX−XXX

to note that catalysts in RWGS and FT reactors are susceptible to deactivation, such as coke poisoning, underscoring the need for a catalyst regeneration unit.

In the C_8-C_{16} range, most FT products are *n*-paraffins with a 1-olefin/*n*-paraffin ratio of 0.1−0.7 mol/mol, as shown in Figure S2.7 of the Supporting Information. However, hydrogenation of these olefins is typically designed to occur after additional steps (FT downstream processing), such as separation of light gases, olefin oligomerization, or hydrocracking. Additionally, this work focuses on C_8-C_{16} products directly from FT synthesis without downstream processing influences. Based on these reasons, a hydrogenation unit immediately after the FT synthesis reactor is not included in the RWGS-FT route.

2.1.4. Second H_2 and CO_2 Separation. Following FT synthesis, the products are cooled and fed to a three-phase separator to separate gas, liquid hydrocarbons, and water products. The liquid hydrocarbons undergo fractionation (not included in this work), while the gas stream containing unreacted H_2, CO, CO_2, and CH_4 product goes to the second H_2 and CO_2 separation unit. The fractionation column yields hydrocarbon cuts in the liquefied petroleum gas, kerosene, diesel, and wax carbon ranges. After the second H_2 and CO_2 separation unit, CO_2 is recycled to the RWGS reactor, while H_2 is recycled to both the RWGS and the FT reactors. The majority of the gas stream, now mainly consisting of unreacted CO, is recycled to the FT reactor. Furthermore, 5% of this stream consisting of CO and CH_4 is purged as off-gas for heat generation, which is utilized at the RWGS preheater (HEATER-1) and the RWGS reactor.

2.2. Methanol Route. In the methanol route, six main stages are considered, as depicted in Figure 1b: (1) direct methanol synthesis from CO_2, (2) methanol purification, (3) MTO conversion, (4) olefin separation, (5) oligomerization, and (6) hydrogenation. Both methanol and light olefins play crucial roles as key intermediates in this route. A detailed process flow diagram of each unit can be found in Section S3.1 of the Supporting Information. Similar to the RWGS-FT route, fractionation is not included in the simulation.

2.2.1. Methanol Synthesis. The direct conversion of CO_2 and H_2 into methanol is primarily driven by methanol synthesis (Reaction 6). However, alongside this main reaction, side reactions such as the RWGS (Reaction 1), ethanol formation (Reaction 7), and dimethyl ether (DME) formation (Reaction 8) can also take place. For simulation purposes, the kinetic model implemented in Aspen Tech's Methanol Synthesis model V12.1[34] was adopted. This model is based on kinetics proposed by Vanden Bussche and Froment,[35] utilizing $Cu/ZnO/Al_2O_3$ as a catalyst, with thermodynamic equilibrium constants provided by Graaf and Winkelman.[36] The kinetics of ethanol and DME formation reactions are derived from studies conducted by Julio et al.[37] and Chiang and Lin,[38] respectively. To ensure accuracy, some rate expression parameters were adjusted to better align with experimental data on C_2H_5OH and DME yields, as documented in the Aspen Tech's Methanol Synthesis model V12.1[34] documentation. Further details regarding the applied kinetic models for the methanol synthesis reactor can be found in Section S3.3 of the Supporting Information.

$$CO_2 + 3H_2 \leftrightarrow CH_3OH + H_2O \quad \Delta H^0 = -49.5\ \text{kJ/mol} \tag{6}$$

$$2CO + 4H_2 \rightarrow C_2H_5OH + H_2O \quad \Delta H^0 = -253.6\ \text{kJ/mol} \tag{7}$$

$$2CH_3OH \rightarrow CH_3OCH_3 + H_2O \quad \Delta H^0 = -23.5\ \text{kJ/mol} \tag{8}$$

The methanol synthesis based on a Cu/ZnO catalyst under operating conditions of 50 bar and 250 °C has shown methane production at ppm levels, which can be managed by a small purge within the gas recycle loop of the methanol synthesis reactor.[39] This insignificant amount of methane is mostly omitted in the literature when discussing methanol synthesis from CO_2.[40−44] Therefore, based on the minimal methane production, this work does not consider methane production in the methanol synthesis reactor.

The reactor (MEOHSYN) is simulated by using a plug flow reactor model, operating at 230 °C and 90 bar. Typically, the molar feed ratio of H_2 to carbon depends on whether CO or CO_2 is used in the feed. For syngas with high CO/CO_2 ratios, a stoichiometric ratio—defined as $S_R = (H_2 - CO_2)/(CO + CO_2)$—higher than 2 is preferred.[45] Higher molar ratios of H_2/CO_2 ranging from 3 to 20[46,47] have been suggested for direct methanol synthesis from CO_2 and H_2. Elevated ratios tend to result in lower concentrations of water byproduct, thereby reducing its adsorption on the catalyst and enhancing methanol synthesis performance while limiting catalyst aging.[45,46,48] In this work, the feed consists of pure CO_2 and H_2 at a 1:3 molar ratio and is compressed to 90 bar using a series of compressors with intercooling. Prior to entering the methanol synthesis reactor, the feed is preheated to 200 °C. Simulated results indicate approximately 20% CO_2 conversion, comparable to that presented in a recent report for direct methanol synthesis from CO_2.[41] The product stream from the reactor is cooled to 35 °C (COOLER-5), after which the liquid product and unreacted gas are flashed (FLASH-1). The unreacted gas is recycled back into the reactor, with a small portion (0.2%) purged to minimize byproduct accumulation in the reaction loop. The liquid product is then directed to the next unit, methanol purification.

2.2.2. Methanol Purification. The liquid stream, termed crude methanol, consists of mainly CH_3OH, water, traces of ethanol and DME, and residual gases. This mixture undergoes expansion to 1.1 bar over a throttle, following which the residual gases are nearly completely removed in a flash tank (FLASH-2). The resulting liquid stream is then heated to 83 °C (HEATER-2) before being fed into the distillation column (MEOHDIST). Methanol, comprising approximately 97 wt % of the mixture, is collected at the top of the column at a temperature of 65.6 °C and atmospheric pressure, while the bottom product, containing water with 0.7 wt % of methanol, exits at 97 °C. Methanol is subsequently directed to the MTO section. In addition, the distillation process can be designed to achieve nearly 100% methanol purity by adjusting parameters such as reflux ratio, bottoms rate, and number of stages. However, this would require more energy for the distillation. A small fraction of water less than 5 wt % in the feed to the MTO reactor showed an insignificant effect on MTO reactivity.[49] Some studies also suggested that a small amount of water in the methanol feed could beneficially prolong catalyst lifetime.[50−52] Therefore, achieving higher methanol purity for MTO is not necessary and could potentially reduce the energy demand and costs in the methanol purification process.

https://doi.org/10.1021/acssuschemeng.4c03939
ACS Sustainable Chem. Eng. XXXX, XXX, XXX−XXX

2.2.3. MTO. Presently, MTO technology has advanced to the point of commercial viability and is in operation, licensed, e.g., by UOP/Hydro and by Dalian Institute of Chemical Physics and Sinopec.[13,14] The overall stoichiometry of MTO reactions is captured in Reaction 9, wherein $[CH_2]$ represents the average oligomeric branch of an olefin hydrocarbon. Operating in the temperature range of 350−550 °C, MTO is a highly exothermic process. Due to strong catalyst coking during MTO reactions, MTO commercial units operate using a fluidized bed reactor coupled with a fluidized bed regenerator, allowing continuous catalyst regeneration and circulation back to the reactor.[13] The reactor outlet typically undergoes cooling for quenching and purification before downstream processing for olefins separation.[21] The quenching and purification steps involve a two-stage process.[53] At this stage, impurities such as catalyst fines and carboxylic acids are eliminated, precipitating with water at the bottom of a quenching tower.[53] The vapor product from the quenching step is subsequently purified, with small amounts of unreacted species and water removed through adsorption using molecular sieves.[53]

Since the simulation cannot account for catalyst fines and carboxylic acids, and considering their exclusion from the applied MTO lumped kinetic model,[49] the quenching and purification steps are omitted and the MTO reactor is modeled using an isothermal plug-flow reactor. The catalyst regeneration units for MTO are not incorporated into the process simulation. Consequently, the energy demand for MTO catalyst regeneration and further steps of quenching and purification are excluded from the results. Nevertheless, carbon loss due to coking and the MTO reactivity affected by coking are included in the implemented kinetic model, as described next.

The kinetic model applied for MTO is derived from the work by Ying et al.,[49] utilizing a fixed bed and fluidized-bed reactor and the SAPO-34 catalyst. In this study, the reactor (MTO) is simplified to an isothermal plug-flow reactor, operated at 490 °C under a pressure of 1 bar. The lumped kinetic model by Ying et al.[49] converts CH_3OH to CH_4, C_2H_4, C_2H_6, C_3H_6, C_3H_8, C_4H_8, C_5H_{10}, and C_6H_{12}, the latter representing coke (Reactions 10−17). Hydrogen addition is necessary for paraffin formation, which can arise from methanol decomposition (Reaction 18) and the WGS reaction (reverse of Reaction 1) at high temperatures. These two reactions are therefore incorporated into the reaction network of the MTO reactor, employing kinetic parameters proposed by Najafabadi et al.[54] MTO commonly faces rapid deactivation due to coke deposition on the catalyst; however, partly plugged pores resulting from coke deposition can enhance selectivity toward light olefins.[13] To streamline the simulation, this study does not include a deactivation model predicting product distribution dependence on coke content; instead, the coke content is fixed at 4.44 wt %[55] in the applied model. This means that the applied kinetic model represents the coke content on the MTO catalyst as a linear function of catalyst residence time, and the olefin product distribution is therefore independent of the coke content. Details of the kinetic model for the MTO reactor are outlined in Section S3.4 of the Supporting Information. The MTO reactor inlet, after mixing with recycled gas stream, is composed of 96.38 wt % CH_3OH, 2.97 wt % H_2O, and small fractions of byproducts, including 0.6 wt % CO_2 and 0.05 wt % C_2H_5OH. The achieved methanol conversion is 99.96%, with a selectivity of 41 and 39 wt % toward C_2H_4 and C_3H_6, respectively.

$$CH_3OH \rightarrow [CH_2] + H_2O \quad (9)$$

$$CH_3OH + H_2 \rightarrow CH_4 + H_2O \quad (10)$$

$$CH_3OH \rightarrow 1/2C_2H_4 + H_2O \quad (11)$$

$$CH_3OH + H_2 \rightarrow 1/2C_2H_6 + H_2O \quad (12)$$

$$CH_3OH \rightarrow 1/3C_3H_6 + H_2O \quad (13)$$

$$CH_3OH + H_2 \rightarrow 1/3C_3H_8 + H_2O \quad (14)$$

$$CH_3OH \rightarrow 1/4C_4H_8 + H_2O \quad (15)$$

$$CH_3OH \rightarrow 1/5C_5H_{10} + H_2O \quad (16)$$

$$CH_3OH \rightarrow 1/6C_6H_{12} + H_2O \quad (17)$$

$$CH_3OH \rightarrow CO + 2H_2 \quad (18)$$

2.2.4. Olefins Separation. Following the MTO reaction, the outlet stream from the MTO reactor (MTO) is cooled to 35 °C (COOLER-7), with the water product separated from gaseous olefin products in a flash tank (FLASH-3). The gas stream is compressed to 10 bar and cooled to 35 °C before entering the distillation column (C_2H_4DIST), where lighter components ($\leq C_2$) and heavier olefins ($\geq C_3$) are separated. The olefins are separated into C_2 and $C_{>2}$ fractions prior to oligomerization because the oligomerization of C_2H_4 and higher olefins is catalyzed by different catalysts. Ni-containing catalysts are required for C_2H_4 oligomerization, while acid-based catalysts are used for the oligomerization of $C_{>2}$ olefins.[56] This study applies a two-stage oligomerization process where C_2H_4 is fed to the first oligomerization reactor with a Ni-based catalyst, while heavier olefins are fed to the second oligomerization reactor, as described in more detail in the Oligomerization part.

Simulation results indicate that the top product comprises roughly 74 wt % C_2H_4 and 24 wt % C_3H_6, while the bottom product contains less than 2×10^{-5} wt % C_2H_4. The primary design objective is to recover nearly all C_2H_4 produced as the top product, with some admixture of C_3H_6 deemed acceptable. The condenser and reboiler of the distillation column operate at −25 and 37 °C, respectively. The distillation column is designed with 10 stages with the feed stream entering above stage 3. It uses a reflux ratio of 1.6 mol base and applies an equilibrium-type calculation method. The top product is directed downstream to the first oligomerization reactor (OLIGO-1), while the bottom product ($\geq C_3$) is routed to the second oligomerization reactor (OLIGO-2).

2.2.5. Oligomerization. The selective conversion of light olefins into jet-fuel-range (C_8−C_{16}) products via oligomerization presents a significant challenge. Olefin oligomerization is typically catalyzed by acid sites using a classical carbenium ion route or by metal sites like Ni via a Cossee-Arlman 1,2 insertion mechanism.[57,58] However, many metal-based catalysts exhibit selectivity toward C_2H_4 feed because of steric hindrance, making it difficult for longer chain olefins to coordinate before insertion.[57,59] To address this, a catalytic cascade reaction has been proposed, involving C_2H_4 oligomerization over metal-based catalysts to produce short to medium chain (C_4−C_{10}) olefins, followed by further oligomerization of these olefins to longer chain olefins within

https://doi.org/10.1021/acssuschemeng.4c03939
ACS Sustainable Chem. Eng. XXXX, XXX, XXX−XXX

the C_8-C_{16} range over acid-based catalysts.[56,60] This cascade oligomerization model is incorporated into the simulation, where two oligomerization reactors are modeled using yield reactors (OLIGO-1 and OLIGO-2). Product yields for each reactor are given based on experimental data from Lacarriere et al.,[56] providing comprehensive C_4-C_{18} olefin product distribution necessary for implementing the distribution of each olefin component in the C_8-C_{16} range. Details of the specified product component yield are outlined in Section S3.5 of the Supporting Information. The top product from the olefin separation unit, primarily composed of C_2H_4 with some C_3H_6, enters the first reactor (OLIGO-1), where the Ni-based catalyst (i.e., Ni-MCM-41) selectively catalyzes mainly into linear C_4 and C_6 olefins, along with small amounts of C_8, C_{10}, and C_{12} olefins. Operating conditions for this reactor are 35 bar and 150 °C. Subsequently, the outlet stream from the first reactor, mixed with the bottom product from the olefin separation unit containing primarily C_3H_6 and C_4H_8, enters the second oligomerization reactor (OLIGO-2). Here, acid-catalyzed co-oligomerization of C_4 or longer olefins over the H-MCM-41 catalyst occurs at 1.5 bar and 150 °C. The products from the second reactor, mainly consisting of C_8-C_{16} olefins, are cooled to 80 °C (COOLER-9), and the gas and liquid products are separated in a flash tank (FLASH-5). The gas stream, primarily containing C_4 and C_6 olefins, is recycled into the second oligomerization reactor, while the liquid stream proceeds downstream to the hydrogenation unit.

2.2.6. Hydrogenation. Olefins, being highly reactive compounds, are prone to forming deposits in jet engines, making it imperative to limit their presence in jet fuel. Hydrogenation, a process aimed at saturating the double bonds of olefins, is essential for jet fuel production for quality assurance. This reaction typically occurs over a solid catalyst and requires an excess feed of H_2 to ensure nearly complete conversion of olefins to paraffins. The hydrogenation reactor is represented in the model using a stoichiometric reactor model (HYDRO), assuming stoichiometric reaction conditions at 15 bar and 320 °C.[61] The H_2/olefins feed ratio is approximately 1:1 (mol-base). The simulation is set to achieve a 95% conversion of olefins. Following hydrogenation, the hydrocarbon products are cooled (COOLER-10) and could undergo further processing (not included in this work), such as fractionation in a column, to separate different cuts, such as light hydrocarbons, jet fuel range hydrocarbons (C_8-C_{16}), and heavier hydrocarbons. Furthermore, olefin oligomerization produces a majority of branched olefins for products beyond C_6.[56] Therefore, processing C_8-C_{16} via the methanol route requires only a hydrogenation step without the need for an isomerization unit within the downstream processing.

For simplification in the process simulation, the catalyst regeneration unit for the oligomerization reactor is not incorporated in this work. However, it is important to note that the catalysts are susceptible to coke poisoning as well as other types of deactivation, such as metal sintering, necessitating the presence of a catalyst regeneration unit.

2.3. CO_2 Electrolysis Route. In this route, C_2H_4 is the key intermediate produced via a CO_2 coelectrolysis process specifically tuned to yield C_2H_4 as the only olefin. Similar to the methanol route, the downstream process of oligomerization, hydrogenation, and hydrocarbon fractionation is required to produce paraffins in the C_8-C_{16} range. The route consists of six main parts, as illustrated in Figure 1c: (1) CO_2 coelectrolysis, (2) CO_2 removal, (3) H_2O removal, (4) C_2H_4 purification, (5) oligomerization, and (6) hydrogenation. A detailed process flow diagram of each unit can be found in Section S4.1 of the Supporting Information.

2.3.1. CO_2 Electrolyzer. The base case was derived from the lab-scale report of CO_2 coelectrolysis using gas diffusion electrodes (GDEs) and a cation exchange membrane to separate the two liquid chambers on the cathode and anode side, avoiding product crossover. The lab-scale results reported by F. Bernasconi et al.[18] (details in Section S4.2 in the Supporting Information) were extrapolated to a larger scale of 100 m^2 electrode active area, corresponding to C_2H_4 production of approximately 0.2 tonnes/day. These quantities should be sufficient to achieve economies of scale for downstream separation processes in C_2H_4 production.[62] The production rates of the other products are also derived from experimental data, as summarized in Table S4.1 in the Supporting Information. In these CO_2 electrolysis cells, the GDEs are positioned between a gas chamber, where the CO_2 reactant flows, and a liquid chamber containing an aqueous electrolyte. Here, the CO_2 electroreduction reaction (CO_2RR) takes place, yielding carbon products (and H_2 as a byproduct). A second liquid chamber, separated from the first with a cation exchange membrane, contains the anode performing the oxygen evolution reaction and is also filled with a aqueous electrolyte.[63,64] Based on the lab-scale results, the use of Cu GDES yields C_2H_4 as the primary gas product, alongside lesser quantities of CH_4 and H_2, with measured Faradaic efficiencies being 50, 10, and 5%, respectively. Ethanol and acetic acid are, instead, the main liquid products, with a Faradaic efficiency of 20 and 10%, respectively. The overall reactions involved are listed in Reactions 19−23. The CO_2 flow rate leaving the cathode was determined by the CO_2 conversion factor, with the anodic CO_2 crossover assumed to be negligible thanks to the presence of the cation exchange membrane. The scale-up simulation assumes a maximum CO_2 conversion of 30%, reflecting the most optimistic case observed in the current lab-scale experiments. As a result, the gas leaving the electrolyzer cathode chamber contains unreacted CO_2 along with C_2H_4, CH_4, and H_2.

$$2CO_2 + 12H^+ + 12e^- \rightarrow C_2H_4 + 4H_2O \quad (19)$$

$$CO_2 + 8H^+ + 8e^- \rightarrow CH_4 + 2H_2O \quad (20)$$

$$2H^+ + 2e^- \rightarrow H_2 \quad (21)$$

$$2CO_2 + 12H^+ + 12e^- \rightarrow C_2H_5OH + 3H_2O \quad (22)$$

$$2CO_2 + 8H^+ + 8e^- \rightarrow C_2H_4O_2 + 2H_2O \quad (23)$$

The focus of this work is on the downstream separation process of the cathode gas outlet stream with the aim to purify C_2H_4 and separate unreacted CO_2 for recycling. This study does not consider any separation process involving the liquid products as C_2H_4 is the sole intermediate of interest for C_8-C_{16} production. Ethanol and acetic acid liquid products are considered as coproducts due to their high market value. It may be more advantageous for this route if electrochemical CO_2RR research could achieve a higher yield of C_2H_4 than the current 50% Faradaic efficiency and reduce the production of other gas and liquid products, rather than requiring additional separation processes to convert ethanol to C_2H_4. However, the economic feasibility of these additional separation and

https://doi.org/10.1021/acssuschemeng.4c03939
ACS Sustainable Chem. Eng. XXXX, XXX, XXX−XXX

conversion processes should be further evaluated through a techno-economic analysis.

Nevertheless, the ethanol in the cathodic liquid product stream could be further separated and dehydrated to form C_2H_4, which could then be fed into the oligomerization process to enhance the yield of C_8-C_{16} hydrocarbons produced by this route. Ethanol can be separated with an approximately 95 wt % purity via double- or triple-column extractive distillation from the azeotropic mixture of H_2O, CH_3COOH, and CH_2O_2.[19,65−67] This is followed by ethanol dehydration to produce C_2H_4. Ethanol dehydration is a mildly endothermic reaction (ΔH^0 = 45.6 kJ/mol) that can be catalyzed by acid-based catalysts such as silica and alumina.[68] The current industrial reactor for C_2H_4 production via ethanol dehydration uses alumina-supported catalysts with an ethanol feed purity of 95 wt %, operating at 300−500 °C and 1−2 bar, achieving a C_2H_4 selectivity of 94−99%.[69,70] Although the ethanol dehydration to C_2H_4 production process is mature, ongoing research focuses on intensifying the process and lowering the operating temperature with further advancements in catalyst design, reactor design, and process optimization.[69,71,72] Furthermore, the dehydration reactor is followed by a two-phase separator, where the gas stream consists of primary crude C_2H_4 and the liquid stream consists of water and ethanol. After this, the crude C_2H_4 must be purified through various stages, including water washing, alkaline washing, drying, and separation in a light-ends tower and a heavy-ends tower to remove light and heavy byproducts.[69] Then, C_2H_4 was sent to the first oligomerization reactor.

2.3.2. CO_2 Removal. In this step, the aim is to separate unreacted CO_2 from the cathode gas stream and recycle it back into the electrolyzer. There are several methods for CO_2 recovery at high TRL such as adsorption, absorption, and membrane-based processes. However, in all these cases, the exact composition of the gas stream needs to be controlled to optimize performance and to not jeopardize adsorbent or membrane materials.[62] The membrane technique, which we previously applied in the RWGS-FT route for CO_2 separation, is an attractive method due to its lower energy demand. However, the current membrane technology might be unable to efficiently separate CO_2 from C_2H_4 and CH_4 due to many similarities in their physicochemical properties, requiring a further careful assessment.[73,74] Thus, we consider the well-established method of CO_2 absorption in aqueous monoethanolamine (MEA) solutions instead.[75,76] The process flow diagram of the CO_2 removal unit is illustrated in Figure S4.1 in the Supporting Information. The CO_2 absorption on MEA is performed at 1 bar and 30 °C, similar conditions to those of the cathode outlet stream. Through the countercurrent contact of the gas and MEA solvent in the absorber (MEA-AB-1), CO_2 is removed from the gas stream. The gas stream without CO_2 leaves at the top of the absorber column and contains C_2H_4, CH_4, H_2, and H_2O, with water being unavoidably transferred from the aqueous MEA solvent. Subsequently, this stream is directed to the next unit for water removal before undergoing cryogenic distillation. The CO_2-rich MEA leaves the absorber at the bottom and then enters the MEA stripping column (MEA-STP), where the MEA solvent is regenerated and recycled into the absorber. The stripper pressure is kept constant at 1.7 bar.[77] The stripper reboiler is kept at approximately 120 °C to avoid thermal degradation of the MEA. The absorber and stripper are modeled using the RadFrac column model. The reaction kinetics and simulation details for the MEA-based CO_2 removal unit are described in Section S4.3 in the Supporting Information. The regenerated MEA solvent leaves as the bottom stream of the stripper, while the CO_2 gas exits as the top stream and is then recycled into the CO_2 electrolyzer.

2.3.3. H_2O Removal. The gas stream after CO_2 removal containing C_2H_4, CH_4, H_2, and water enters the H_2O removal unit, where the triethylene glycol-based (TEG) dehydration process takes place. Water must be removed prior to the C_2H_4 purification unit to avoid freezing during cryogenic distillation, where lighter gases H_2 and CH_4 will be further separated from C_2H_4. The TEG dehydration unit is similar to the MEA unit and consists of an absorber (TEG-AB) and a stripper (TEG-STP). The TEG absorber is operated at 40 bar.[78] The gaseous feed stream is compressed to 40 bar and cooled down to 50 °C, at which point the stream remains in the gas phase and then flows into the TEG absorber at the bottom of the column. The dehydrated gas stream, leaving the top of absorber, is sent to the cryogenic distillation unit for C_2H_4 purification. The water-rich TEG stream is sent to the stripper in which TEG solvent is regenerated and water is separated, leaving at the top of the stripper. The stripper reboiler is kept at 203−204 °C to avoid TEG thermal degradation taking place at above 206 °C. The regenerated TEG leaves the stripper with a purity of 98.61 wt %; thus, a makeup TEG is needed to achieve 99 wt % as required for the absorber. The simulation details for the TEG-based H_2O removal unit are described in Section S4.4 in the Supporting Information.

2.3.4. C_2H_4 Purification. Cryogenic distillation is applied for separating light gases. The gas stream exits the TEG-based dehydration unit containing light gases: 3.6 wt % of H_2, 14.1 wt % of CH_4, and 82.3 wt % of C_2H_4. This stream is then compressed to 240 bar to facilitate the initial Joule-Thomson cooling of H_2 gas prior to it entering the cryogenic distillation column (CRYODIST). To achieve this H_2 cooling effect, the stream should be below its inversion temperature of around −73 °C. The cryogenic distillation achieves 99.99 wt % C_2H_4 purity flowing out as the bottom product, while the gas stream at the top is composed of H_2 19.86 wt % and CH_4 78.96 wt %. A further separation of H_2 and CH_4 gases could be performed by PSA or membrane techniques similar to that applied in H_2 production from steam-methane reforming.[79] Alternatively, this H_2 and CH_4 gas mixture can be used as a fuel to cover heating requirements within the process. In this work, further separation of H_2 and CH_4 gases is not included. The total C_2H_4 loss during the downstream separation process is minimal (0.42% by mass). The simulation details of cryogenic distillation are described in Section S4.5 in the Supporting Information. In addition, the gas mixture exiting the H_2O removal unit containing a small fraction of 3.6 wt % of H_2 could be alternatively removed by adsorption or membrane techniques instead of cryogenic distillation.[79] However, when mixed with C_2H_4 and CH_4 gases, further careful assessment is needed.

Based on our lab-scale CO_2 co-electrolysis experimental results, CO is not reported as one of the main gas products because of its insignificant amount with less than 5% Faradaic efficiency. While several works reported relatively higher amount of CO gas product from CO_2 electrolysis,[80,81] this fact likely depends on the applied current density. An optimal current density for C_2H_4 production leads to minimization of the quantity of CO as this product is further reduced to C_2H_4.[18,82] Moreover, CO may not have a significant impact in

https://doi.org/10.1021/acssuschemeng.4c03939
ACS Sustainable Chem. Eng. XXXX, XXX, XXX−XXX

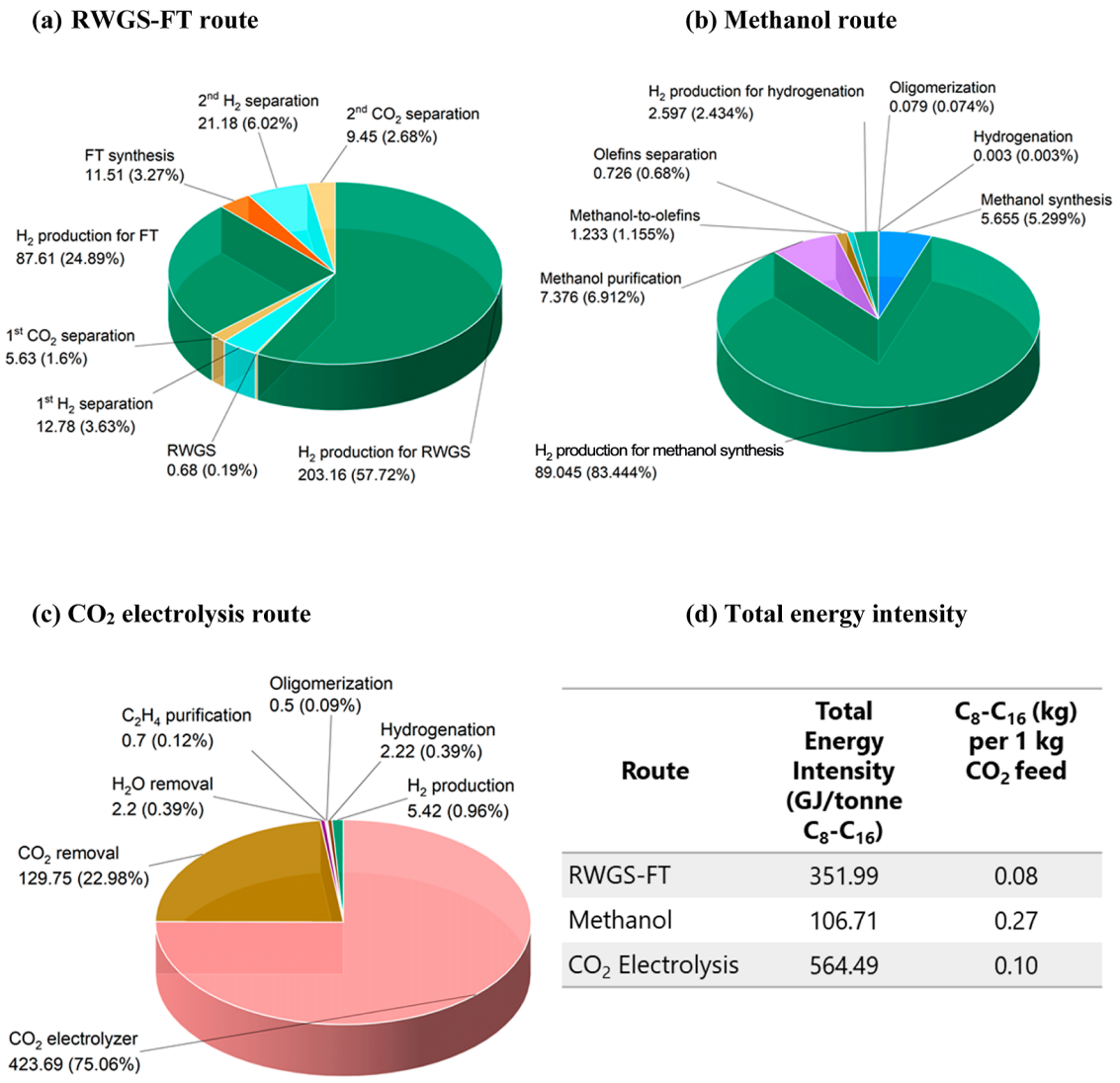

Route	Total Energy Intensity (GJ/tonne C_8-C_{16})	C_8-C_{16} (kg) per 1 kg CO_2 feed
RWGS-FT	351.99	0.08
Methanol	106.71	0.27
CO_2 Electrolysis	564.49	0.10

Figure 2. Energy intensity in GJ/tonne C_8−C_{16} of each unit in (a) RWGS-FT route, (b) methanol route, and (c) CO_2 electrolysis route and (d) total energy intensity and C_8−C_{16} yield of each route.

the downstream process because it would be removed during cryogenic distillation together with H_2 and CH_4, with slight changes in energy demand for this unit.

The high purity of C_2H_4 achieved after distillation (99.99 wt %) allows, in principle, its use as a precursor for polymer production. Nevertheless, here we focus on C_2H_4 as a key intermediate in the synthesis of hydrocarbons in the C_8−C_{16} range; thus, we continue with considering an ethylene oligomerization unit.

2.3.5. Oligomerization and Hydrogenation. Similar to the methanol route, the electrochemically produced C_2H_4 is fed to the first oligomerization reactor (OLIGO-1) operating at 35 bar, 150 °C, followed by the second oligomerization reactor (OLIGO-2) operating at 1 bar, 150 °C, to obtain longer chain olefins. Downstream, olefins are hydrogenated in the hydrogenation reactor (HYDRO) operating at 15 bar and 320 °C with assumed 95% conversion to paraffins. The simulation details of the oligomerization and hydrogenation units are described in Section S4.5 in the Supporting Information.

It should be noted that the presence of CH_4 alongside C_2H_4 in the feed is not expected to influence the oligomerization process due to the relatively low reactivity of CH_4 compared to that of C_2H_4. Nevertheless, the presence of H_2 in the feed could lead to early C_2H_4 hydrogenation in the oligomerization reactor, particularly under high-pressure conditions. This would result in lower oligomerization reactivity and a reduced yield of longer chain olefins. Therefore, we identify the suppression of H_2 production during CO_2 electrolysis as a key future development that will potentially reduce the need for any downstream H_2-separation process (e.g., cryogenic distillation), leading to significant reductions in both energy and capital costs.

3. ENERGY INTENSITY

In this section, we explore the energy demand of the three routes, which includes electrical, heating, and cooling loads. Electrical energy is primarily used for water and CO_2 electrolyzers and rotating equipment such as compressors and pumps. Heating is required for providing adequate conversion temperatures and loads for reactors as well as for separation units, such as reboilers at strippers and distillation columns. Cooling is primarily needed for rotating and separation equipment (interstage cooling of compressors, condensers at distillation columns, and strippers) and reactors

https://doi.org/10.1021/acssuschemeng.4c03939
ACS Sustainable Chem. Eng. XXXX, XXX, XXX−XXX

for exothermic reactions, as well as for reactor output streams. Typically, the energy input for cooling loads tends to be lower than that for heating loads. Cooling, below ambient temperatures, requires electrical energy for compression chillers.

First, this study considers possible heat exchange between hot and cold streams within each process to account for possible internal heat recovery (detailed heat integration analysis in Section S5.2 of the Supporting Information). Subsequently, the remaining heating and cooling loads are translated into their equivalent electrical energy demands. The remaining required heating loads are assumed to be supplied through Joule heating at 100% efficiency. Cooling loads necessitated for cooling to temperatures above 35 °C are presumed to be achieved by cooling water at ambient temperature (25 °C), whereas cooling to below 35 °C requires cooling water from a compression chiller. A coefficient of performance of 5[83] for compression chillers is applied for cooling below 35 °C. This signifies that for every 5 kWh of cooling, 1 kWh of electricity is supplied for heat removal. This work does not factor in electrical energy supply to pumps required for cooling water circulation for the cooling to temperature above 35 °C.[83] Finally, considering potential heat exchange and the energy input for heating and cooling loads, as described, the energy input required for the three routes is calculated within the selected boundaries. Additionally, Section S5.1 of the Supporting Information presents data on the total heating and cooling loads in each unit of the three routes without considering heat integration and the conversion of heating and cooling loads to electrical energy demand as mentioned above.

To calculate the energy intensity (GJ/tonne C_8-C_{16}) of the three pathways, the production rates of the target hydrocarbons C_8-C_{16} are extracted from the output stream of the hydrogenation reactor in the methanol (MEO-18) and CO_2 electrolysis routes (ELO-17) and from the liquid product stream of the FT reactor in the RWGS-FT route (FT-38). This ensures an accurate assessment of total C_8-C_{16} production for each route without being influenced by variations in the downstream fractionation design. Here, the energy input for producing green H_2 is determined by using an energy efficiency of the water electrolyzer of 70% based on the lower heating value (LHV) of H_2. The efficiency of water electrolysis using advanced alkaline or proton exchange membrane electrolysis may vary between 60 and 77%.[84]

Utilizing potential heat integration and the assumptions described above, Figure 2 illustrates the required electric energy input of each unit per metric ton (tonne) of products in the range of C_8-C_{16} (energy intensity) from the three routes. The total energy intensity, as depicted in Figure 2d, reveals that the methanol route requires approximately 3.5 times less electrical energy than the RWGS-FT route, while the CO_2 electrolysis route shows the highest energy intensity. H_2 production accounts for the largest portion of energy input for both the methanol (about 83%) and RWGS-FT routes (also about 83%), whereas the CO_2 electrolyzer accounts for the largest portion in the CO_2 electrolysis route, i.e., approximately 75% of the energy input.

Product selectivity (Figure 3a) and C_8-C_{16} yield (Figure 2d) also play crucial roles in the process energy intensity evaluation. Bube et al.[21] reported a kerosene selectivity of 61−77% for the RWGS-FT pathway and 60−90% for the methanol pathway. This study reports C_8-C_{16} selectivity of 48% (mole) for the RWGS-FT pathway and 83% (mole) for the methanol

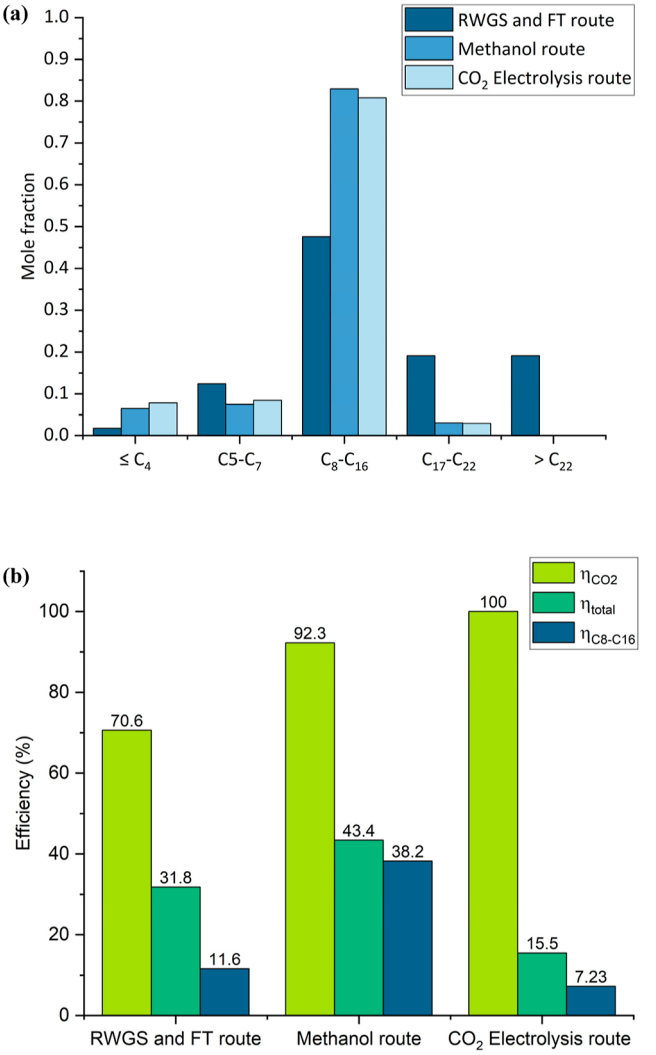

Figure 3. Comparison of (a) production distribution and (b) CO_2 efficiency, η_{Co2}, total thermal efficiency, η_{total}, and C_8-C_{16} fraction thermal efficiency, $\eta_{C_8-C_{16}}$, of the RWGS-FT route, methanol route, and CO_2 electrolysis route.

pathway (Figure 3a). Bube et al.[21] used the Anderson−Schulz−Flory (ASF) distribution to model FT synthesis products and included the hydrocracking downstream process. In contrast, the study at hand excludes hydrocracking process and uses the kinetic model by Todic et al.,[32] which describes FT synthesis products that commonly deviate from ASF distribution, showing higher methane yields, lower C_2 yields (particularly C_2H_4), and decreasing slopes in the ASF diagram with increasing carbon number. Furthermore, Bube et al.[21] used a generic ASF distribution with one-stage oligomerization for the methanol pathway, while this study implemented two-stage oligomerization and modeled product yield based on experimental results. Methodological differences in simulating product distribution contribute to deviations in the reported results. Here, kinetic models derived from experimental results were selected to predict product distribution more accurately, matching experimental results in key reactions. Higher selectivity toward C_8-C_{16} is observed for the methanol and CO_2 electrolysis routes, with the best C_8-C_{16} yield occurring in the methanol route. Each route is discussed in more detail in the following sections.

https://doi.org/10.1021/acssuschemeng.4c03939
ACS Sustainable Chem. Eng. XXXX, XXX, XXX−XXX

3.1. RWGS-FT Route. The H_2 production makes up the biggest share, approximately 83%, of the total energy demand of the RWGS-FT route, as shown in Figure 2a. 25% of the total energy demand is needed for the production of H_2 to feed the FT reactor. This constitutes approximately 32% of total H_2 entering the FT reactor, with the rest being recycled H_2. The energy intensity associated with recycling H_2 is reflected in the H_2 separation units, which are significant (around 10%), while that of the CO_2 separation units is approximately 4%. The higher energy input in H_2 separation units is due to the relatively high operating pressure of 40 bar for the PSA process. This suggests that reducing the H_2/CO ratio required for optimal CO conversion and higher productions of long carbon chain products (C_{5+}) of FT reactions[85] could diminish the amount of H_2 to be separated and subsequently lower the energy requirement at the second H_2 separation unit. Additionally, while PSA techniques are widely used in the oil and gas industry, employing low-pressure H_2 separation technologies such as membrane separation for H_2 separation from the gas mixture in the RWGS and FT processes could significantly reduce the energy intensity in this route. However, the components of the gas mixture should be carefully assessed for the viability of this method.[86,87]

Moreover, 70% of the total H_2 is required for the RWGS reaction, contributing to the immense energetic effort for the CO_2 reduction within this subprocess. Despite considerable efforts to comprehend the RWGS process across different scales, it is yet to be realized at an industrial scale.[11] The development of efficient catalysts exhibiting higher activity and stability, alongside optimized reactor designs and potential strategies to address the sluggish kinetics and to lower the reaction temperature of the RWGS, remain critical challenges in advancing the industrial applicability of this process.[11,88] In the simulation at hand, 5 wt % of the off-gas from the gas product stream post-FT reactor is harnessed to generate energy for heating loads at the preheater of the RWGS reactor (HEATER-1) and within the RWGS reactor itself (Figure S5.7a in the Supporting Information). This off-gas utilization helps to keep the energy input to the RWGS unit in Figure 2a relatively small, despite the high temperature of 800 °C. This purged stream also adversely impacts the CO_2 efficiency of the RWGS-FT route. The detailed heat integration of this route is shown in Figure S5.7 in the Supporting Information.

The selectivity for the desired product range significantly impacts the product-specific energy intensity. Given that the FT synthesis produces a wide range of hydrocarbons, optimizing this route for C_8−C_{16} production remains a critical challenge. Designing tailored catalysts to enhance selectivity toward distillates in the C_8−C_{16} range is essential for tackling this challenge.[89,90]

The energy intensity of the CO_2 reduction in the RWGS process and its low technical maturity as well as the low selectivity of the FT process and downstream hydrogen separation pose significant challenges in the RWGS-FT route. The detailed investigation of the impact of the endothermic high-temperature RWGS process will be discussed in Section. 5.

3.2. Methanol Route. The primary energy requirement is from green H_2 production for methanol synthesis (83.4%), followed by distillation to separate methanol from water (6.9%), and the methanol synthesis unit itself (5.3%), mainly for compression to the high reaction pressure (Figure 2b). The energy intensity shown in Figure 2b already accounts for the heat integration that could be implemented in the methanol synthesis, MTO, oligomerization, and hydrogenation units, where most hot streams exiting the reactors are used to provide heat for preheating of cold streams (detailed in Figure S5.8 in the Supporting Information). Additionally, heat from combustion of purge streams is considered. Downstream of the methanol synthesis reactor, there are two purge streams: PURGED-1 and PURGED-2, containing mostly H_2 and CO_2 and little CO. The combination of the two purge streams results in a heat supply of ($\dot{m} \times$ LHV) of 112.39 GJ/h, which is sufficient to supply the reboiler operating at 97 °C at the methanol distillation column requiring 104.09 GJ/h (detailed in Figure S5.8b in the Supporting Information). These necessary purges reduce the carbon efficiency of this pathway, which is discussed in the next section. Alternatively, the PURGE-2 stream can also be compressed and recycled into the methanol reactor. Another option is to send the product stream of the methanol reactor to another distillation column to remove residual light components such as H_2, CO_2, and CO[91] before proceeding to the methanol−water distillation column. Both will inevitably increase the energy demand of the methanol route.

Although the energy supply at the methanol distillation reboiler can be partially provided by combustion of purged gas, the energy required for the methanol purification unit remains substantial, with approximately 7% of the total energy intensity (Figure 2b). This is attributed to the preheating required before the methanol−water distillation. The relatively high energy intensity of the methanol synthesis results from high-pressure (90 bar) operation conditions of the reactor. This highlights a need for advanced catalysts and reactor design for promoting methanol synthesis at lower pressure while also increasing CO_2 conversion to minimize the need for CO_2 recycle efforts as well as increasing methanol yield.[92] Additionally, improving methanol yield by removing the byproduct water during the reaction, which is the focus of ongoing research,[93−97] is a promising approach. This method could simultaneously reduce energy input at the methanol purification unit and increase the downstream hydrocarbon product yield, thereby lowering the energy intensity of the process.

Furthermore, the MTO process, oligomerization, and hydrogenation also require relatively high operating temperatures, but these are exothermic reactions. The reactors themselves do not contribute to the energy demand when heat integration is considered (detailed in Figure S5.8c−h in the Supporting Information). Additionally, well-designed olefin oligomerization favors C_8−C_{16} production (0.8 mole fraction), compared to FT synthesis, which produces a significant share of higher chain hydrocarbons (>C_{16}) resulting in a notably lower share of C_8−C_{16} (roughly 0.4 mole fraction) (Figure 3a). This high selectivity to C_8−C_{16}, along with the high yield of C_8−C_{16} (Figure 2d) by oligomerization, significantly contributes to the lower energy intensity in the methanol routes compared to the RWGS-FT route. This highlights the potential of utilizing oligomerization technology and the methanol route for industrial applicability. Nevertheless, coking of the catalyst in MTO and oligomerization significantly reduces hydrocarbon product yields while also resulting in carbon and hydrogen losses and a reduction in process efficiency.[98,99]

The methanol route exhibits relatively low energy intensity, attributed to its high selectivity and potential heat-self-

https://doi.org/10.1021/acssuschemeng.4c03939
ACS Sustainable Chem. Eng. XXXX, XXX, XXX−XXX

sufficiency. However, challenges remain, particularly in methanol synthesis from CO_2 and the coking issues observed in MTO and oligomerization processes. The effect of coking in MTO is investigated and is discussed further in Section 5. Additionally, the technical maturity of the direct conversion of CO_2 to methanol and the oligomerization process aimed at producing C_8-C_{16} are currently low.

3.3. CO_2 Electrolysis Route. In the CO_2 electrolysis route, the primary energy demand is attributed to the CO_2 electrolyzer, accounting for 75% of the total energy demand (Figure 2c). This calculation is based on a cell voltage of 4.5 V at 0.2 A/cm^2, which is scaled up to a total of 100 m^2. In the best-case scenario from our lab-scale experiment, the cell voltage can be reduced to 3.2 V, resulting in a lower energy requirement of 301 GJ/tonne C_8-C_{16} (68%). Furthermore, considering the thermodynamic cell voltage of 1.15 V required to produce ethylene, the energy demand decreases to 108.3 GJ/tonne C_8-C_{16} (43.5%), indicating substantial room for improvement in cell efficiency. The impact of reducing cell voltage is discussed in more detail in Section 5. Note also that in the electrolyzer, CO_2 reduction is paired with H_2O-oxidation (O_2 evolution), with the latter responsible for more than 60% of the energy consumption associated with the process. Substituting this anodic reaction with one requiring lower voltage and yielding valuable products would substantially mitigate the energy impact of the electrolysis step.

Approximately 23% of the total energy demand is attributed to CO_2 removal from the product stream of the CO_2 electrolyzer, primarily needed by the MEA stripper reboiler for MEA regeneration (Table S5.3 in the Supporting Information). This energy demand strongly depends on CO_2 conversion at the electrolyzer, a topic that will be investigated and discussed in Section 5. However, it is important to note that our analysis focuses on downstream energy requirements for C_8-C_{16} production, assuming that the CO_2 separation downstream of the anode tail gas due to anodic CO_2 crossover and carbonate formation is negligible. Thus, all unreacted CO_2 in the electrolyzer is assumed to exit the cathode and be further removed in the CO_2 separation unit. However, it is worth noting that the energy input for separating CO_2 in the anode tail gas could also be significant if the loss of CO_2 to the anode is substantial. Alerte et al. reported that with the assumption of 0.5 mol CO_2/mol e^- of anodic CO_2 crossover, CO_2 in the anode tail gas could account for approximately four times the amount of CO_2 exiting the cathode for a single-pass CO_2 conversion of 25%.[62] Furthermore, the energy intensity reported in Figure 2c does not include the separation processes of the CO_2 electrolyzer liquid products, i.e., ethanol and acetic acid, nor does it include the separation between H_2 and CH_4 gas products. Alternatively, after the cryogenic distillation had left as the top product, the H_2 gas could be purified and utilized at the downstream hydrogenation unit, while the CH_4 gas could be combusted to generate heat within the process.

The energy intensity at the water removal, cryogenic distillation, oligomerization, and hydrogenation units is relatively low. Similar to the methanol route, the heat exchange between the outlet and inlet streams of the reactors can be exploited in the oligomerization and hydrogenation unit (detailed in Figure S5.9 in the Supporting Information).

Furthermore, the high-pressure operation at the first oligomerization reactor (OLIGO-1), which operates at 35 bar, may contribute to the higher energy requirements at the oligomerization unit in the CO_2 electrolysis route compared to those in the methanol route. In the methanol route, approximately 41 wt % of olefins produced via MTO is C_2H_4, while the remainder consists of olefins in the C_3-C_5 range. These are directly fed to the second oligomerization reactor (OLIGO-2), which operates at a pressure of 1 bar. This suggests that selectively producing higher olefin chains such as C_3H_6 and C_4H_8 through the MTO process, where their oligomerization reactions can occur at lower pressure, would help reduce energy consumption at the oligomerization unit.

4. PROCESS EFFICIENCY

Three metrics, total thermal efficiency (considering the C_1-C_{30} range of synthetic crude hydrocarbons), C_8-C_{16} fraction thermal efficiency, and CO_2 efficiency, are employed to further evaluate and compare the three routes. Carbon efficiency, η_{Co_2}, which represents the CO_2 to synthetic crude (C_1-C_{30}) conversion efficiency, total thermal efficiency, η_{total}, which denotes the electrical energy to synthetic crude conversion efficiency, and the C_8-C_{16} fraction thermal efficiency, $\eta_{C_8-C_{16}}$, which represents the efficiency of the conversion of electrical energy to the C_8-C_{16} fraction are calculated using eqs 24–26, respectively. The CO_2 efficiency is

$$\eta_{CO_2} = \frac{\dot{n}_{\text{feed}CO_2} - \dot{n}_{\text{purged}CO_2}}{\dot{n}_{\text{feed}CO_2}} \tag{24}$$

where $\dot{n}$ denotes the molar flow rate and $\dot{n}_{\text{purged}CO_2}$ is the summation of CO_2 molar flow rates embodied in all purged streams after complete oxidation.

The total thermal efficiency considering the crude as product is

$$\eta_{total} = \left[(\dot{m}h_{LHV,\leq C_4}) + (\dot{m}h_{LHV,C_5-C_7}) + (\dot{m}h_{LHV,C_8-C_{16}}) + (\dot{m}h_{LHV,C_{17}-C_{22}}) + (\dot{m}h_{LHV,C_{22+}})\right]/P_{el} \tag{25}$$

and the thermal efficiency only considering the C_8-C_{16} fraction as product is

$$\eta_{C_8-C_{16}} = \frac{\dot{m}h_{LHV,C_8-C_{16}}}{P_{el}} \tag{26}$$

where $\dot{m}h_{LHV,frac}$ is the enthalpy flow rate (GJ/h) of a product considering its LHV. P_{el} represents the electrical power (GJ/h) needed for combined technical work for compression, heating, and cooling to operate the entire process route. The CO_2 and enthalpy flows of each synthetic crude oil division of the three routes are provided in Table S6.1 in the Supporting Information. The results of the three metrics for the three routes are depicted in Figure 3b.

The RWGS-FT route exhibits the lowest CO_2 efficiency, at 70.6%, primarily due to the utilization of purged streams for heating loads at the RWGS reactor and preheater (HEATER-1). In contrast, the two purged streams in the methanol route are significantly smaller, resulting in a higher CO_2 efficiency of 92.2%. Bube et al.[21] reported a total carbon efficiency of 74–92% for the methanol pathway where major carbon losses occur during the methanol-to-kerosene conversion due to limited selectivity in dehydration of olefins and olefins oligomerization. The post-MTO process differs, with Bube et al.[21] including catalyst regeneration and dehydration, while our study uses distillation to separate olefins into C_2 and $C_{>2}$, followed by two-stage oligomerization. Additionally, the

https://doi.org/10.1021/acssuschemeng.4c03939
ACS Sustainable Chem. Eng. XXXX, XXX, XXX−XXX

carbon loss modeling in the literature's dehydration step is unclear. The differences in post-MTO separation and oligomerization processes contribute to the deviation in the carbon efficiency. In this study, carbon losses in the methanol pathway include losses in the MTO reactor and purge stream.

The CO_2 electrolysis route has the potential to achieve close to 100% CO_2 efficiency, provided that the light gas, consisting of 79 wt % CH_4 and 20 wt % H_2, which serves as the top product at cryogenic distillation, can be effectively purified and utilized for other value-added chemicals production. Various techniques, such as PSA, dense palladium-based membranes, and polymeric, ceramic, and carbon membranes, can be employed for H_2 separation from CH_4 gas mixtures.[100] The CO_2 efficiency reduces to 94.8% if CH_4 is considered to be a waste stream due to its low value.

In terms of the total thermal efficiency of conversion of CO_2 to synthetic crude, the methanol route demonstrates the highest efficiency at 43.4%, surpassing the RWGS-FT route at 31.8%, while the CO_2 electrolysis route exhibits the lowest efficiency at 15.5%. Previous reports on the total efficiency of the RWGS and FT synthesis to produce fuels range from 31 to 41% by Hannula et al.[8] and 55−60% by Zang et al.[101] The differences may stem from various factors in the detailed process modeling setup. These include variations in the RWGS temperature, ranging from 600 to 800 °C, methods for providing heat to the RWGS, as well as differences in the H_2/CO_2 feed ratio to the RWGS reactor. Additionally, variations exist in the modeling approach for FT synthesis to estimate the product distribution. Differences can also be found in CO_2 and H_2 separation techniques, as well as the inclusion of FT product upgrading units such as hydro-processing of wax components. The design of the CO/H_2 recycle placement within the FT recycle loop is another factor that varies. Efficiency assessment of H_2 produced from water electrolysis based on the LHV varies in the literature ranging from 60 to 100%.

The methanol route exhibits the highest efficiency for C_8−C_{16} production, $\eta_{C_8-C_{16}}$ (38.2%), nearly matching its total thermal efficiency. This suggests that the methanol route holds significant potential for sustainable jet fuel production compared with the other two routes. The considerable drop in thermal efficiency seen in the CO_2 electrolysis route can be attributed to the notably high energy intensity of the overall processes and the relatively low selectivity toward C_2H_4 by CO_2 electrolysis. Ethylene, the primary intermediate produced by the CO_2 electrolyzer for hydrocarbon fuel production, accounts for only about 50% of the yield at the electrolyzer. Another valuable liquid product, i.e., ethanol, requires an additional dehydration unit to produce C_2H_4, which would entail further energy input. Therefore, enhancing the C_2H_4 yield is crucial for optimizing this route for sustainable jet fuel production as well.

5. INFLUENCE OF KEY PROCESS FACTORS ON ENERGY INTENSITY AND EFFICIENCY

In this section, we explore the influence of several previously identified key processes on energy intensity and process efficiency. This includes the absence of off-gas combustion for heating energy in the RWGS unit within the RWGS-FT route, coke production in the MTO reactor within the methanol route, and the CO_2 electrolyzer cell voltage and CO_2 conversion in the CO_2 electrolysis route.

Without the energy supplied by off-gas combustion to the RWGS unit, the total CO_2 efficiency of the RWGS-FT route could potentially reach 100%, which is consistent with those reported by Bube et al.[21] However, the energy intensity of the RWGS-FT route increases significantly by 21.32 GJ/tonne C_8−C_{16} (6.07%) as electrical heating is necessary, as shown in Table 1. Although the CO_2 efficiency has the potential to reach 100%, $\eta_{C_8-C_{16}}$ remains similar and does not change significantly (roughly 1%). This option should consider the trade-off between the energy increase and the associated energy demand for CO_2 capture resulting from combustion, alongside the potential utilization of light gases, predominantly CH_4, produced from the FT route as value-added chemicals.

Table 1. Comparison of Total Energy Intensity, CO_2 Efficiency, and Thermal Efficiency of the C_8−C_{16} Fraction between Scenarios with and without Off-Gas Combustion in the RWGS-FT Route

	total energy intensity (GJ/tonne C_8−C_{16})	η_{co_2} (%)	$\eta_{C_8-C_{16}}$ (%)
Inclusion of off-gas combustion (base case)	351.99	70.61	11.59
Without off-gas combustion	373.31	100	10.93

One critical key process, identified in the methanol route, is catalyst coking in the MTO step. The critical factors for the operation of this unit are coke production and product selectivity. Coke production has a 2-fold influence on the process: the current coke content in the catalyst impacts the methanol conversion, while coke production and removal translate into a loss in hydrocarbon products and carbon efficiency.

The implemented kinetic model, illustrated in Figure S3.7 (Section S3.4 in the Supporting Information), shows that exceeding 6 wt % of coke in the MTO catalyst leads to a significant decrease in methanol conversion. For example, with a coke content of 7.5 wt %, methanol conversion drops to 59%, resulting in a reduced yield of C_8−C_{16} products (reduced by 40% by mass). This, in turn, leads to a lower $\eta_{C_8-C_{16}}$ (23%) and a significantly higher energy intensity, as shown in Figure 4a. This is primarily due to an increase in the energy intensity of downstream units by 14−66%, as illustrated in Figure 4b. This highlights the critical challenge posed by coking issues on the performance and efficiency of the MTO step, emphasizing the necessity of addressing this issue for process improvement. Recently, extensive research is focusing on catalyst coking in MTO to achieve a long lifetime of its catalysts.[51,102] In case coke production could be limited while keeping the performance of a state-of-the-art catalyst (simulated with the previously presented kinetic model with a constant coke content of 4.4 wt %), the energy intensity of the methanol route with respect to C_8−C_{16} products could be reduced by 4% (102.37 GJ/tonne C_8−C_{16}) through the increased production of C_8−C_{16}. This increases the efficiency of $\eta_{C_8-C_{16}}$ by 1.6% (Figure 4a) while reducing carbon losses.

For the CO_2 electrolysis route, the impact of reducing the CO_2 electrolyzer cell voltage and increasing the CO_2 conversion is given in Figure 5a,b, respectively. Reducing the cell voltage shows a constant rate of change in the CO_2 electrolyzer's energy demand for a constant product output. For the theoretical limiting voltage for the reduction of CO_2 to

https://doi.org/10.1021/acssuschemeng.4c03939
ACS Sustainable Chem. Eng. XXXX, XXX, XXX−XXX

(a)

	Total energy intensity (GJ/tonne C8-C16)	η_{C8-C16} (%)
Coke 4.4 wt% (base case)	106.71	38.22
Coke 7.5 wt%	177.30	23.00
Coke production stop at 4.4 wt%	102.37	39.84

(b)

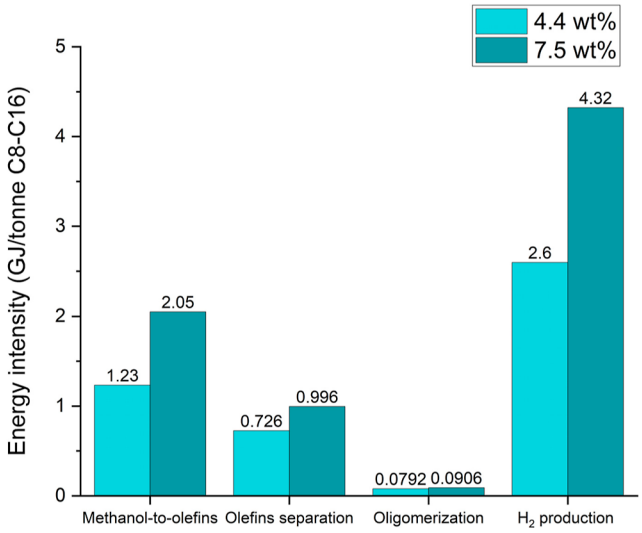

Figure 4. (a) Comparison of total energy intensity and thermal efficiency of the C_8-C_{16} fraction between scenarios with different coke production levels at the MTO reactor in the methanol route. (b) Energy intensity of downstream process units when the coke content at the MTO reactor is 4.4 and 7.5 wt %.

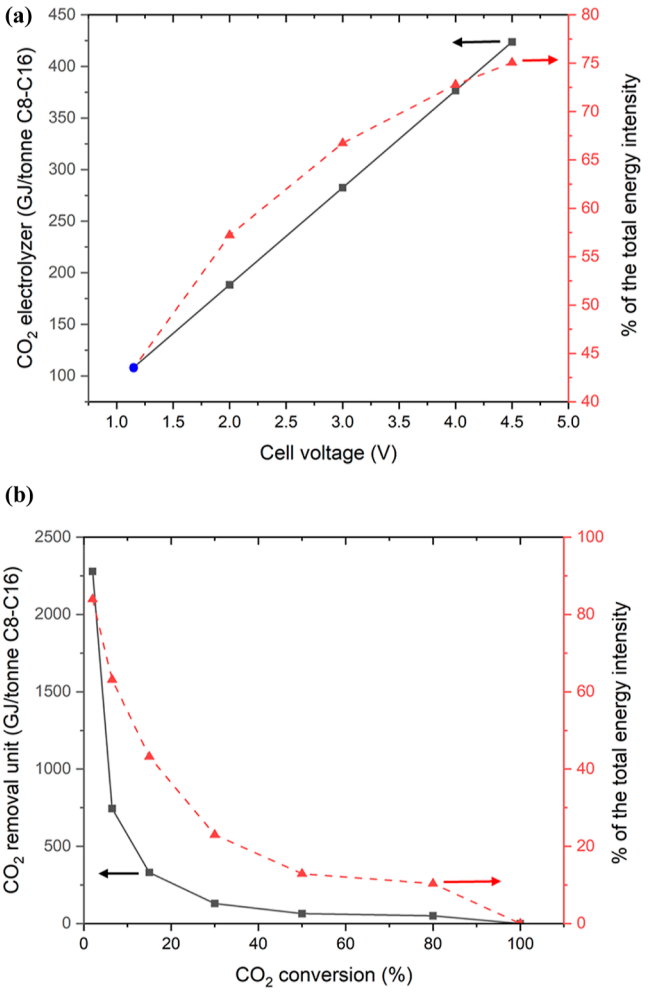

Figure 5. Unit energy intensity and its percentage of the total energy intensity: (a) the CO_2 electrolyzer unit, varying with cell voltage, where the blue circle represents the data at the theoretical voltage of CO_2 reduction to ethylene at 1.12 V, and (b) the CO_2 removal unit, varying with CO_2 conversion.

C_2H_4, the electrolyzer would still account for 44% of the total energy intensity with respect to C_8-C_{16} products (based on 30% CO_2 conversion).

Increasing the level of CO_2 conversion within the electrolyzer results in an exponential reduction in the energy demand for the removal of CO_2 from the electrolyzer's product stream. This is significant up to 40−50% CO_2 conversion, beyond which the influence on the overall energy intensity becomes smaller. At a cell voltage of 4.5 V, CO_2 conversions in the electrolyzer below approximately 15% lead to the CO_2 removal unit dominating the energy demand of the total process, exceeding the energy demand of the electrolyzer itself.

6. CONCLUSIONS

In this work, we investigated pathways for the production of sustainable liquid hydrocarbons in the C_8-C_{16} range, key components of jet fuels, directly from CO_2, with the aim of providing guidance for research and development efforts. The aim is to facilitate the transition of the aviation industry away from fossil fuels and toward achieving near-term emission reduction goals. As most direct CO_2 utilization technologies are currently at low technological maturity, the identification of promising pathways is key to sustainable process development. This study investigates three pathways for jet fuel production, represented by hydrocarbons in the C_8-C_{16} range. The three routes utilize key catalytic processes for direct CO_2 conversion into different key intermediate compounds, i.e., syngas, methanol, and ethylene via the RWGS-FT route, methanol route, and CO_2 electrolysis route, respectively. Results are obtained through comprehensive process modeling and utilizing the available literature and lab-scale data, and they offer an early-stage evaluation of emerging CO_2 to jet fuel technologies and identification of key technical development needs for chemical conversion technologies in each route.

The findings suggest that the energy intensity of the C_8-C_{16} product of the methanol route is the lowest, followed by the RWGS-FT and the CO_2 electrolysis routes, which are approximately 3.5 and 5 times higher, respectively. While the RWGS-FT route demonstrates the lowest CO_2 efficiency due to the utilization of off-gas combustion for heating loads of the RWGS reactor, the methanol route shows significantly higher CO_2 efficiency, reaching 92%, indicating its effectiveness in utilizing the CO_2 feedstock. Moreover, the methanol route exhibits the highest thermal efficiency, targeting the C_8-C_{16} range as well. These results highlight the promising potential of the methanol route for sustainable jet fuel production. The CO_2 electrolysis route currently lags in energy efficiency

https://doi.org/10.1021/acssuschemeng.4c03939
ACS Sustainable Chem. Eng. XXXX, XXX, XXX−XXX

attributed to its high energy intensity and relatively low selectivity toward ethylene of the CO_2 electrolysis step.

The RWGS-FT route has the highest technology readiness but exhibits substantial energy intensity, with H_2 production representing the predominant share. Strategies such as enhancing FT conversion and reducing the H_2/CO feed ratio without compromising the conversion can potentially reduce H_2 demand, increase hydrocarbon products, and mitigate energy demand at the downstream H_2 separation unit. Employing low-pressure H_2 separation techniques also presents a promising avenue for reducing the energy intensity. However, additional challenges persist, including the elevated temperature of RWGS, which poses a 6% higher energy intensity without utilizing heat from off-gas combustion, emphasizing the importance of efficient heat integration in this route and hindering the attainment of 100% of the CO_2 efficiency to hydrocarbon products. Furthermore, the wide array of hydrocarbon products from FT synthesis signifies the need for catalyst development aimed at higher selectivity in the C_8−C_{16} range for jet fuel production. Another approach could involve process design tailored toward longer hydrocarbon chains, followed by hydrocracking for C_8−C_{16} production. However, the associated energy and H_2 feedstock demands need to be assessed in relation to the trade-off for selective production.

The methanol route offers promising avenues for enhancing energy efficiency in C_8−C_{16} production compared with the other two routes. H_2 production constitutes the largest share of the energy intensity in this route. Challenges include the low technological maturity of direct CO_2 to methanol conversion and issues with catalyst coking in MTO and oligomerization, which require further developments in both catalysts and process efficiency for industrial applicability. Moreover, ongoing research focusing on improving the methanol yield by removing water during methanol synthesis could be promising in mitigating the substantial energy demand of downstream methanol−water distillation while increasing methanol production. The high operating pressure required for direct CO_2 conversion to methanol requires advancements in reactor and process development to promote the reaction at lower pressures without compromising CO_2 conversion rates. However, the route's high selectivity to C_8−C_{16} hydrocarbons through oligomerization contributes to its lower energy intensity compared to alternative routes, as does the heat self-sufficiency in key process steps, such as methanol synthesis, oligomerization, and hydrogenation, further highlighting the route's viability.

The CO_2 electrolysis route presents both challenges and opportunities for improving the energy efficiency in C_8−C_{16} production. The primary energy demand is attributed to the CO_2 electrolyzer. Lowering the cell voltage, substituting the anodic H_2O-oxidation with one requiring lower voltage and/or yielding a valuable product, and enhancing C_2H_4 yield will reduce the energy impact of the electrolyzer. Additionally, as CO_2 removal from the electrolyzer gas product stream is a significantly energy-intensive process, improvements in CO_2 conversion up to 40−50% will mitigate the energy requirements. Future developments focusing on suppressing H_2 production during electrolysis could eliminate the need for a downstream H_2 separation process, leading to significant energy and cost savings. Furthermore, similar to the methanol route, the potential heat self-sufficiency in oligomerization and hydrogenation, coupled with the highly selective production of higher olefin chains through the oligomerization process, offers promising avenues for enhancing the overall process efficiency. Nevertheless, addressing the challenges in catalyst development to achieve selectivity at C_8−C_{16} and stability in oligomerization is crucial.

While challenges remain in realizing these pathways at an industrial scale, identifying areas for further research and development efforts that could substantially impact process efficiency and reduce energy demand holds promise for advancing sustainable jet fuel production from CO_2 feedstock and contributing to the decarbonization of the aviation industry. Additionally, conducting an overall assessment in terms of production cost, techno-economic considerations, environmental impact, and lifecycle analysis is essential as a next step to gain a comprehensive understanding of the examined pathway's potential.

■ ASSOCIATED CONTENT

Supporting Information

The Supporting Information is available free of charge at https://pubs.acs.org/doi/10.1021/acssuschemeng.4c03939.

Additional details including process diagrams, unit model parameters, reaction kinetics, heat integration, data for energy intensity analysis, and data for CO_2 and thermal efficiency calculations (PDF)

■ AUTHOR INFORMATION

Corresponding Authors

Pussana Hirunsit − *Empa, Swiss Federal Laboratories for Materials Science and Technology, Chemical Energy Carriers and Vehicle Systems Laboratory, 8600 Dübendorf, Switzerland;* orcid.org/0000-0003-1309-7553; Email: pussana.hirunsit@empa.ch

Florian Kiefer − *Empa, Swiss Federal Laboratories for Materials Science and Technology, Chemical Energy Carriers and Vehicle Systems Laboratory, 8600 Dübendorf, Switzerland;* orcid.org/0000-0002-6956-5179; Email: florian.kiefer@empa.ch

Authors

Alessandro Senocrate − *Empa, Swiss Federal Laboratories for Materials Science and Technology, Materials for Energy Conversion Laboratory, 8600 Dübendorf, Switzerland;* orcid.org/0000-0002-0952-0948

Carlos E. Gómez-Camacho − *Empa, Swiss Federal Laboratories for Materials Science and Technology, Technology and Society Laboratory, 9014 St. Gallen, Switzerland;* orcid.org/0000-0002-1982-3598

Complete contact information is available at: https://pubs.acs.org/10.1021/acssuschemeng.4c03939

Notes

The authors declare no competing financial interest.

■ ACKNOWLEDGMENTS

This work was supported by the ETH Board in the framework of the Joint Strategic Initiative "Synthetic Fuels from Renewable Resources". Additionally, parts of this research were carried out with the support of the Swiss Federal Office of Energy as part of the SWEET consortium reFuel.ch. The authors are solely responsible for the conclusions and the results presented in this publication.

REFERENCES

(1) Sacchi, R.; Becattini, V.; Gabrielli, P.; Cox, B.; Dirnaichner, A.; Bauer, C.; Mazzotti, M. How to make climate-neutral aviation fly. *Nat. Commun.* **2023**, *14*, 3989.

(2) IATA (International Air Transport Association). *2022 SAF Production Increases 200% - More Incentives Needed to Reach Net Zero*, 2022. https://www.iata.org/en/pressroom/2022-releases/2022-12-07-01/.

(3) PwC Strategy& (Germany). *From Feedstock to Flight-How to Unlock the Potential of SAF*, 2024. www.strategyand.pwc.com.

(4) *Producing Sustainable Aviation Fuel*. https://aviationbenefits.org/environmental-efficiency/climate-action/sustainable-aviation-fuel/producing-sustainable-aviation-fuel/.

(5) *Directive (EU) 2023/2413 of the European Parliament and of the Council of 18 October 2023 Amending Directive (EU) 2018/2001, Regulation (EU) 2018/1999 and Directive 98/70/EC as Regards the Promotion of Energy from Renewable Sources, and Repealing Council Directive (EU) 2015/652*. https://eur-lex.europa.eu/eli/dir/2023/2413/oj.

(6) Cardiff University, UK. *Regulation (EU) 2023/2405 on Ensuring a Level Playing Field for Sustainable Air Transport (ReFuelEU Aviation)*. https://www.europeansources.info/record/proposal-for-a-regulation-on-ensuring-a-level-playing-field-for-sustainable-air-transport/.

(7) De Klerk, A.; Chauhan, G.; Halmenschlager, C.; Link, F.; Montoya Sánchez, N.; Gartley, B.; Sayed, H. E. M.; Sehdev, R.; Lehoux, R. Sustainable aviation fuel: Pathways to fully formulated synthetic jet fuel via Fischer−Tropsch synthesis. *Energy Sci. Eng.* **2023**, *12*, 394−409.

(8) Hannula, I.; Kaisalo, N.; Simell, P. Preparation of Synthesis Gas from CO2 for Fischer−Tropsch Synthesis—Comparison of Alternative Process Configurations. *C* **2020**, *6*, 55.

(9) Dimitriou, I.; García-Gutiérrez, P.; Elder, R. H.; Cuéllar-Franca, R. M.; Azapagic, A.; Allen, R. W. K. Carbon dioxide utilisation for production of transport fuels: process and economic analysis. *Energy Environ. Sci.* **2015**, *8*, 1775−1789.

(10) Peters, R.; Wegener, N.; Samsun, R. C.; Schorn, F.; Riese, J.; Grünewald, M.; Stolten, D. A Techno-Economic Assessment of Fischer−Tropsch Fuels Based on Syngas from Co-Electrolysis. *Processes* **2022**, *10*, 699.

(11) González-Castaño, M.; Dorneanu, B.; Arellano-García, H. The reverse water gas shift reaction: a process systems engineering perspective. *React. Chem. Eng.* **2021**, *6*, 954−976.

(12) Triviño, M. L. T.; Arriola, N. C.; Kang, Y. S.; Seo, J. G. Transforming CO2 to valuable feedstocks: Emerging catalytic and technological advances for the reverse water gas shift reaction. *Chem. Eng. J.* **2024**, *487*, 150369.

(13) Tian, P.; Wei, Y.; Ye, M.; Liu, Z. Methanol to Olefins (MTO): From Fundamentals to Commercialization. *ACS Catal.* **2015**, *5*, 1922−1938.

(14) Gogate, M. R. Methanol-to-olefins process technology: current status and future prospects. *Pet. Sci. Technol.* **2019**, *37*, 559−565.

(15) Keil, F. J. Methanol-to-hydrocarbons: process technology. *Microporous Mesoporous Mater.* **1999**, *29*, 49−66.

(16) Berkelaar, L.; Linde, J. v. d.; Peper, J.; Rajhans, A.; Tiemessen, D.; Ham, L. v. d.; Berg, H. v. d. Electrochemical conversion of carbon dioxide to ethylene: Plant design, evaluation and prospects for the future. *Chem. Eng. Res. Des.* **2022**, *182*, 194−206.

(17) Chen, Y.; Miao, R. K.; Yu, C.; Sinton, D.; Xie, K.; Sargent, E. H. Catalyst design for electrochemical CO2 reduction to ethylene. *Matter* **2024**, *7*, 25−37.

(18) Bernasconi, F.; Senocrate, A.; Kraus, P.; Battaglia, C. Enhancing $C_{\geq 2}$ product selectivity in electrochemical CO_2 reduction by controlling the microstructure of gas diffusion electrodes. *EES. Catal.* **2023**, *1*, 1009−1016.

(19) Alerte, T.; Gaona, A.; Edwards, J. P.; Gabardo, C. M.; O'Brien, C. P.; Wicks, J.; Bonnenfant, L.; Rasouli, A. S.; Young, D.; Abed, J.; et al. Scale-Dependent Techno-Economic Analysis of CO_2 Capture and Electroreduction to Ethylene. *ACS Sustainable Chem. Eng.* **2023**, *11*, 15651−15662.

(20) Atsonios, K.; Li, J.; Inglezakis, V. J. Process analysis and comparative assessment of advanced thermochemical pathways for e-kerosene production. *Energy* **2023**, *278*, 127868.

(21) Bube, S.; Bullerdiek, N.; Voß, S.; Kaltschmitt, M. Kerosene production from power-based syngas - A technical comparison of the Fischer−Tropsch and methanol pathway. *Fuel* **2024**, *366*, 131269.

(22) Kaiser, P.; Unde, R. B.; Kern, C.; Jess, A. Production of Liquid Hydrocarbons with CO_2 as Carbon Source based on Reverse Water-Gas Shift and Fischer−Tropsch Synthesis. *Chem. Ing. Tech.* **2013**, *85*, 489−499.

(23) Wittich, K.; Krämer, M.; Bottke, N.; Schunk, S. A. Catalytic Dry Reforming of Methane: Insights from Model Systems. *ChemCatChem* **2020**, *12*, 2130−2147.

(24) Bown, R. M.; Joyce, M.; Zhang, Q.; Reina, T. R.; Duyar, M. S. Identifying Commercial Opportunities for the Reverse Water Gas Shift Reaction. *Energy Technol.* **2021**, *9*, 2100554.

(25) Gandara-Loe, J.; Portillo, E.; Odriozola, J. A.; Reina, T. R.; Pastor-Pérez, L. K-Promoted Ni-Based Catalysts for Gas-Phase CO2 Conversion: Catalysts Design and Process Modelling Validation. *Front. Chem.* **2021**, *9*, 785571.

(26) Portillo, E.; Gandara-Loe, J.; Reina, T. R.; Pastor-Pérez, L. Is the RWGS a viable route for CO2 conversion to added value products? A techno-economic study to understand the optimal RWGS conditions. *Sci. Total Environ.* **2023**, *857*, 159394.

(27) Le Saché, E.; Pastor-Pérez, L.; Haycock, B. J.; Villora-Picó, J. J.; Sepúlveda-Escribano, A.; Reina, T. R. Switchable Catalysts for Chemical CO_2 Recycling: A Step Forward in the Methanation and Reverse Water-Gas Shift Reactions. *ACS Sustainable Chem. Eng.* **2020**, *8*, 4614−4622.

(28) Ebrahimi, P.; Kumar, A.; Khraisheh, M. A Review of CeO2 Supported Catalysts for CO2 Reduction to CO through the Reverse Water Gas Shift Reaction. *Catalysts* **2022**, *12*, 1101.

(29) Chen, X.; Chen, Y.; Song, C.; Ji, P.; Wang, N.; Wang, W.; Cui, L. Recent Advances in Supported Metal Catalysts and Oxide Catalysts for the Reverse Water-Gas Shift Reaction. *Front. Chem.* **2020**, *8*, 709.

(30) Morosanu, E. A.; Saldivia, A.; Antonini, M.; Bensaid, S. Process Modeling of an Innovative Power to LNG Demonstration Plant. *Energy Fuels* **2018**, *32*, 8868−8879.

(31) Rytter, E.; Tsakoumis, N. E.; Holmen, A. On the selectivity to higher hydrocarbons in Co-based Fischer−Tropsch synthesis. *Catal. Today* **2016**, *261*, 3−16.

(32) Todic, B.; Bhatelia, T.; Froment, G. F.; Ma, W.; Jacobs, G.; Davis, B. H.; Bukur, D. B. Kinetic Model of Fischer−Tropsch Synthesis in a Slurry Reactor on Co-Re/Al_2O_3 Catalyst. *Ind. Eng. Chem. Res.* **2013**, *52*, 669−679.

(33) Ma, W.; Shafer, W. D.; Martinelli, M. Fischer−Tropsch Reactions and Product Distribution Suits for Downstream. In *Chemicals and Fuels from Biomass via Fischer−Tropsch Synthesis*; Gorimbo, J., Liu, X., Yao, Y., Hildebrandt, D., Eds.; The Royal Society of Chemistry, 2022; pp 188−213..

(34) *Aspen Plus V12.1. Aspen Plus Methanol Synthesis Model*, 2021.

(35) Bussche, K. M. V.; Froment, G. F. A Steady-State Kinetic Model for Methanol Synthesis and the Water Gas Shift Reaction on a Commercial Cu/ZnO/Al2O3Catalyst. *J. Catal.* **1996**, *161*, 1−10.

(36) Graaf, G. H.; Winkelman, J. G. M. Chemical Equilibria in Methanol Synthesis Including the Water-Gas Shift Reaction: A Critical Reassessment. *Ind. Eng. Chem. Res.* **2016**, *55*, 5854−5864.

(37) Julio, M.; Gustavo, P.; Harvey, A.-G.; Rubens, M. F.; Regina, W. M. Syngas to higher alcohols using cu-based catalyst a simulation approach. *Chem. Eng. Trans.* **2015**, *43*, 1519−1524.

(38) Chiang, C.-L.; Lin, K.-S. Preparation and characterization of CuO Al 2 O 3 catalyst for dimethyl ether production via methanol dehydration. *Int. J. Hydrogen Energy* **2017**, *42*, 23526−23538.

(39) Ushikoshi, K.; Mori, K.; Kubota, T.; Watanabe, T.; Saito, M. Methanol synthesis from CO_2 and H_2 in a bench-scale test plant. *Appl. Organomet. Chem.* **2000**, *14*, 819−825.

(40) Lacerda De Oliveira Campos, B.; John, K.; Beeskow, P.; Herrera Delgado, K.; Pitter, S.; Dahmen, N.; Sauer, J. A Detailed Process and Techno-Economic Analysis of Methanol Synthesis from

https://doi.org/10.1021/acssuschemeng.4c03939
ACS Sustainable Chem. Eng. XXXX, XXX, XXX−XXX

H2 and CO2 with Intermediate Condensation Steps. *Processes* **2022**, *10*, 1535.
(41) Poto, S.; Vico Van Berkel, D.; Gallucci, F.; Fernanda Neira d'Angelo, M. Kinetic modelling of the methanol synthesis from CO2 and H2 over a CuO/CeO2/ZrO2 catalyst: The role of CO2 and CO hydrogenation. *Chem. Eng. J.* **2022**, *435*, 134946.
(42) Guil-López, R.; Mota, N.; Llorente, J.; Millán, E.; Pawelec, B.; Fierro, J.; Navarro, R. M. Methanol Synthesis from CO2: A Review of the Latest Developments in Heterogeneous Catalysis. *Materials* **2019**, *12*, 3902.
(43) Marlin, D. S.; Sarron, E.; Sigurbjörnsson, O. ·. Process Advantages of Direct CO2 to Methanol Synthesis. *Front. Chem.* **2018**, *6*, 446.
(44) Bowker, M. Methanol Synthesis from CO $_2$ Hydrogenation. *ChemCatChem* **2019**, *11*, 4238−4246.
(45) Hankin, A.; Shah, N. Process exploration and assessment for the production of methanol and dimethyl ether from carbon dioxide and water. *Sustainable Energy Fuels* **2017**, *1*, 1541−1556.
(46) Tatsumi, M.; Tsukasa, H.; Daisuke, F. *Process for Producing Methanol*, 2013.
(47) Arthur, M.; Shulenberger; Fridrik Ragnar, J.; Oddur, I.; Kim-Chinh, T. Process for Producing Liquid Fuel from Carbon doxde and Water. U.S. Patent 8,198,338 B2, 2007.
(48) Haid, J.; Koss, U. Lurgi's Mega-Methanol technology opens the door for a new era in down-stream applications. in *Natural Gas Conversion VI*; Elsevier, 2001; Vol. *136*, 399−404 .
(49) Ying, L.; Yuan, X.; Ye, M.; Cheng, Y.; Li, X.; Liu, Z. A seven lumped kinetic model for industrial catalyst in DMTO process. *Chem. Eng. Res. Des.* **2015**, *100*, 179−191.
(50) Yang, L.; Wang, C.; Zhang, L.; Dai, W.; Chu, Y.; Xu, J.; Wu, G.; Gao, M.; Liu, W.; Xu, Z.; et al. Stabilizing the framework of SAPO-34 zeolite toward long-term methanol-to-olefins conversion. *Nat. Commun.* **2021**, *12*, 4661.
(51) Valecillos, J.; Elordi, G.; Aguayo, A. T.; Castaño, P. The intrinsic effect of co-feeding water on the formation of active/deactivating species in the methanol-to-hydrocarbons reaction on ZSM-5 zeolite. *Catal. Sci. Technol.* **2021**, *11*, 1269−1281.
(52) Luo, M.; Fu, Y.; Hu, B.; Wang, D.; Wang, B.; Mao, G. Water inhibits the conversion and coking of olefins on SAPO-34. *Appl. Catal., A* **2019**, *570*, 209−217.
(53) Miller, L. W.; Senetar, J. J.. Two-Stage Quench Tower for Use with Oxygenate Conversion Process. U.S. Patent 6,459,009 B1, 2002.
(54) Najafabadi, A. T.; Fatemi, S.; Sohrabi, M.; Salmasi, M. Kinetic modeling and optimization of the operating condition of MTO process on SAPO-34 catalyst. *J. Ind. Eng. Chem.* **2012**, *18*, 29−37.
(55) Yu, B.; Chien, I. Design and Optimization of the Methanol-to-Olefin Process. Part I: Steady-State Design and Optimization. *Chem. Eng. Technol.* **2016**, *39*, 2293−2303.
(56) Lacarriere, A.; Robin, J.; Świerczyński, D.; Finiels, A.; Fajula, F.; Luck, F.; Hulea, V. Distillate-Range Products from Non-Oil-Based Sources by Catalytic Cascade Reactions. *ChemSusChem* **2012**, *5*, 1787−1792.
(57) Nicholas, C. P. Applications of light olefin oligomerization to the production of fuels and chemicals. *Appl. Catal., A* **2017**, *543*, 82−97.
(58) Arlman, E. Ziegler-Natta catalysis III. Stereospecific polymerization of propene with the catalyst system TiCl3$z.sbnd;AlEt3. *J. Catal.* **1964**, *3*, 99−104.
(59) Svejda, S. A.; Brookhart, M. Ethylene Oligomerization and Propylene Dimerization Using Cationic (α-Diimine)nickel(II) Catalysts. *Organometallics* **1999**, *18*, 65−74.
(60) Babu, B. H.; Lee, M.; Hwang, D. W.; Kim, Y.; Chae, H.-J. An integrated process for production of jet-fuel range olefins from ethylene using Ni-AlSBA-15 and Amberlyst-35 catalysts. *Appl. Catal., A* **2017**, *530*, 48−55.
(61) Lilga, M. A. et al. Systems and Processes for Conversion of Ethylene Feedstocks to Hydrocarbon Fuels. U.S. Patent 20,160,194,257 A1, 2018.
(62) Alerte, T.; Edwards, J. P.; Gabardo, C. M.; O'Brien, C. P.; Gaona, A.; Wicks, J.; Obradović, A.; Sarkar, A.; Jaffer, S. A.; MacLean, H. L.; et al. Downstream of the CO $_2$ Electrolyzer: Assessing the Energy Intensity of Product Separation. *ACS Energy Lett.* **2021**, *6*, 4405−4412.
(63) Herranz, J.; Pătru, A.; Fabbri, E.; Schmidt, T. J. Co-electrolysis of CO2 and H2O: From electrode reactions to cell-level development. *Curr. Opin. Electrochem.* **2020**, *23*, 89−95.
(64) Gabardo, C. M.; O'Brien, C. P.; Edwards, J. P.; McCallum, C.; Xu, Y.; Dinh, C. T.; Li, J.; Sargent, E. H.; Sinton, D. Continuous Carbon Dioxide Electroreduction to Concentrated Multi-carbon Products Using a Membrane Electrode Assembly. *Joule* **2019**, *3*, 2777−2791.
(65) Küüt, A.; Ritslaid, K.; Küüt, K.; Ilves, R.; Olt, J. State of the Art on the Conventional Processes for Ethanol Production. In *Ethanol*; Elsevier, 2019; pp 61−101..
(66) Li, G.; Bai, P. New Operation Strategy for Separation of Ethanol-Water by Extractive Distillation. *Ind. Eng. Chem. Res.* **2012**, *51*, 2723−2729.
(67) Yang, A.; Zou, H.; Chien, I. L.; Wang, D.; Wei, S.; Ren, J.; Shen, W. Optimal Design and Effective Control of Triple-Column Extractive Distillation for Separating Ethyl Acetate/Ethanol/Water with Multiazeotrope. *Ind. Eng. Chem. Res.* **2019**, *58*, 7265−7283.
(68) Gärtner, C. A.; van Veen, A. C.; Lercher, J. A. Oxidative Dehydrogenation of Ethane: Common Principles and Mechanistic Aspects. *ChemCatChem* **2013**, *5*, 3196−3217.
(69) Zhang, M.; Yu, Y. Dehydration of Ethanol to Ethylene. *Ind. Eng. Chem. Res.* **2013**, *52*, 9505−9514.
(70) Chauhan, R.; Sartape, R.; Minocha, N.; Goyal, I.; Singh, M. R. Advancements in Environmentally Sustainable Technologies for Ethylene Production. *Energy Fuels* **2023**, *37*, 12589−12622.
(71) Ouayloul, L.; Agirrezabal-Telleria, I.; Arias, P. L.; Dumeignil, F.; Doukkali, M. E. Tuning the Acid Nature of the ZSM-5 Surface for Selective Production of Ethylene from Ethanol at Low Temperatures. *Energy Fuels* **2024**, *38*, 4492−4503.
(72) Gao, Y.; Neal, L.; Ding, D.; Wu, W.; Baroi, C.; Gaffney, A. M.; Li, F. Recent Advances in Intensified Ethylene Production—A Review. *ACS Catal.* **2019**, *9*, 8592−8621.
(73) Bachman, J. E.; Reed, D. A.; Kapelewski, M. T.; Chachra, G.; Jonnavittula, D.; Radaelli, G.; Long, J. R. Enabling alternative ethylene production through its selective adsorption in the metal-organic framework Mn $_2$ (*m* -dobdc). *Energy Environ. Sci.* **2018**, *11*, 2423−2431.
(74) Chen, K.-J.; Madden, D. G.; Mukherjee, S.; Pham, T.; Forrest, K. A.; Kumar, A.; Space, B.; Kong, J.; Zhang, Q. Y.; Zaworotko, M. J. Synergistic sorbent separation for one-step ethylene purification from a four-component mixture. *Science* **2019**, *366*, 241−246.
(75) Wang, Y.; Zhao, L.; Otto, A.; Robinius, M.; Stolten, D. A Review of Post-combustion CO2 Capture Technologies from Coal-fired Power Plants. *Energy Procedia* **2017**, *114*, 650−665.
(76) D'Alessandro, D. M.; Smit, B.; Long, J. R. Carbon Dioxide Capture: Prospects for New Materials. *Angew. Chem., Int. Ed.* **2010**, *49*, 6058−6082.
(77) Rezazadeh, F.; Gale, W. F.; Lin, Y.-J.; Rochelle, G. T. Energy Performance of Advanced Reboiled and Flash Stripper Configurations for CO $_2$ Capture Using Monoethanolamine. *Ind. Eng. Chem. Res.* **2016**, *55*, 4622−4631.
(78) Chebbi, R.; Qasim, M.; Abdel Jabbar, N. Optimization of triethylene glycol dehydration of natural gas. *Energ Rep.* **2019**, *5*, 723−732.
(79) Sircar, S. Pressure Swing Adsorption. *Ind. Eng. Chem. Res.* **2002**, *41*, 1389−1392.
(80) Ajmal, S.; Yasin, G.; Kumar, A.; Tabish, M.; Ibraheem, S.; Sammed, K. A.; Mushtaq, M. A.; Saad, A.; Mo, Z.; Zhao, W. A disquisition on CO2 electroreduction to C2H4: An engineering and design perspective looking beyond novel choosy catalyst materials. *Coord. Chem. Rev.* **2023**, *485*, 215099.
(81) Fan, M.; Huang, J. E.; Miao, R. K.; Mao, Y.; Ou, P.; Li, F.; Li, X. Y.; Cao, Y.; Zhang, Z.; Zhang, J.; et al. Cationic-group-functionalized

https://doi.org/10.1021/acssuschemeng.4c03939
ACS Sustainable Chem. Eng. XXXX, XXX, XXX−XXX

electrocatalysts enable stable acidic CO2 electrolysis. *Nat. Catal.* **2023**, *6*, 763−772.
(82) García De Arquer, F. P.; Dinh, C. T.; Ozden, A.; Wicks, J.; McCallum, C.; Kirmani, A. R.; Nam, D. H.; Gabardo, C.; Seifitokaldani, A.; Wang, X.; et al. CO $_2$ electrolysis to multicarbon products at activities greater than 1 A cm $^{-2}$. *Science* **2020**, *367*, 661−666.
(83) Architectural Energy Corporation, Boulder, CO. *Design Brief: Chiller Plant Efficiency*. https://datacenters.lbl.gov/sites/default/files/Design%20Brief_Chiller%20Efficiency.pdf.
(84) Smolinka, T. Fuels−Hydrogen Production | Water Electrolysis. In *Encyclopedia of Electrochemical Power Sources*; Elsevier, 2009; pp 394−413..
(85) Ostadi, M.; Rytter, E.; Hillestad, M. Boosting carbon efficiency of the biomass to liquid process with hydrogen from power: The effect of H2/CO ratio to the Fischer−Tropsch reactors on the production and power consumption. *Biomass Bioenergy* **2019**, *127*, 105282.
(86) David, O. C.; Gorri, D.; Urtiaga, A.; Ortiz, I. Mixed gas separation study for the hydrogen recovery from H2/CO/N2/CO2 post combustion mixtures using a Matrimid membrane. *J. Membr. Sci.* **2011**, *378*, 359−368.
(87) Salim, W.; Ho, W. S. W. Hydrogen purification with CO2-selective facilitated transport membranes. *Curr. Opin. Chem. Eng.* **2018**, *21*, 96−102.
(88) Su, X.; Yang, X.; Zhao, B.; Huang, Y. Designing of highly selective and high-temperature endurable RWGS heterogeneous catalysts: recent advances and the future directions. *J. Energy Chem.* **2017**, *26*, 854−867.
(89) Sharifnia, S.; Mortazavi, Y.; Khodadadi, A. Enhancement of distillate selectivity in Fischer−Tropsch synthesis on a Co/SiO2 catalyst by hydrogen distribution along a fixed-bed reactor. *Fuel Process. Technol.* **2005**, *86*, 1253−1264.
(90) Westphalen, G.; Cortez, K. A.; Baldanza, M. A. S.; de Almeida, A. J.; Salim, V. M. M.; da Silva, M. A. P.; da Silva, V. T. High Selectivity of Medium Distillates in Fischer−Tropsch Synthesis Using Dual Bed. *Catal. Lett.* **2022**, *152*, 2533−2542.
(91) Borisut, P.; Nuchitprasittichai, A. Methanol Production via CO2 Hydrogenation: Sensitivity Analysis and Simulation—Based Optimization. *Front. Energy Res.* **2019**, *7*, 81.
(92) Dieterich, V.; Buttler, A.; Hanel, A.; Spliethoff, H.; Fendt, S. Power-to-liquid *via* synthesis of methanol, DME or Fischer−Tropsch-fuels: a review. *Energy Environ. Sci.* **2020**, *13*, 3207−3252.
(93) Terreni, J.; Trottmann, M.; Franken, T.; Heel, A.; Borgschulte, A. Sorption-Enhanced Methanol Synthesis. *Energy Technol.* **2019**, *7*, 1801093.
(94) Maksimov, P.; Nieminen, H.; Laari, A.; Koiranen, T. Sorption enhanced carbon dioxide hydrogenation to methanol: Process design and optimization. *Chem. Eng. Sci.* **2022**, *252*, 117498.
(95) Seshimo, M.; Liu, B.; Lee, H. R.; Yogo, K.; Yamaguchi, Y.; Shigaki, N.; Mogi, Y.; Kita, H.; Nakao, S. i. Membrane Reactor for Methanol Synthesis Using Si-Rich LTA Zeolite Membrane. *Membranes* **2021**, *11*, 505.
(96) Li, Z.; Tsotsis, T. T. Methanol synthesis in a high-pressure membrane reactor with liquid sweep. *J. Membr. Sci.* **2019**, *570−571*, 103−111.
(97) Bos, M. J.; Brilman, D. W. F. A novel condensation reactor for efficient CO2 to methanol conversion for storage of renewable electric energy. *Chem. Eng. J.* **2015**, *278*, 527−532.
(98) Mohamed, H. O.; Abed, O.; Zambrano, N.; Castaño, P.; Hita, I. A Zeolite-Based Cascade System to Produce Jet Fuel from Ethylene Oligomerization. *Ind. Eng. Chem. Res.* **2022**, *61*, 15880.
(99) Yu, B.; Zhang, W.; Wei, Y.; Wu, X.; Sun, T.; Fan, B.; Xu, S.; Liu, Z. Capture and identification of coke precursors to elucidate the deactivation route of the methanol-to-olefin process over H-SAPO-34. *Chem. Commun.* **2020**, *56*, 8063−8066.
(100) Lider, A.; Kudiiarov, V.; Kurdyumov, N.; Lyu, J.; Koptsev, M.; Travitzky, N.; Hotza, D. Materials and techniques for hydrogen separation from methane-containing gas mixtures. *Int. J. Hydrogen Energy* **2023**, *48*, 28390−28411.
(101) Zang, G.; Sun, P.; Elgowainy, A. A.; Bafana, A.; Wang, M. Performance and cost analysis of liquid fuel production from H2 and CO2 based on the Fischer−Tropsch process. *J. CO2 Util.* **2021**, *46*, 101459.
(102) Zhao, X.; Li, J.; Tian, P.; Wang, L.; Li, X.; Lin, S.; Guo, X.; Liu, Z. Achieving a Superlong Lifetime in the Zeolite-Catalyzed MTO Reaction under High Pressure: Synergistic Effect of Hydrogen and Water. *ACS Catal.* **2019**, *9*, 3017−3025.

https://doi.org/10.1021/acssuschemeng.4c03939
ACS Sustainable Chem. Eng. XXXX, XXX, XXX−XXX